# Chem Soc Rev

## Correlating concerted cation on oxygen redox in rechargeable batteries

| Journal: | *Chemical Society Reviews* |
|---|---|
| Manuscript ID | CS-SYN-07-2023-000550.R2 |
| Article Type: | Review Article |
| Date Submitted by the Author: | 17-Jan-2024 |
| Complete List of Authors: | Wang, Shiqi; University of Science and Technology Beijing Wang, Lifan; University of Science and Technology Beijing, Department of Physical Chemistry Sandoval, David; Argonne National Laboratory Liu, Tongchao; Argonne National Laboratory, Chemical Science and Engineering Division Zhan, Chun; University of Science and Technology Beijing, Physical Chemistry Amine, Khalil; Argonne National Laboratory |
| | |

SCHOLARONE™
Manuscripts

# Correlating concerted cation on oxygen redox in rechargeable batteries

Shiqi Wang[a], Lifan Wang[a], Sandoval David [b], Tongchao Liu*[b], Chun Zhan*[a] and Khalil Amine*[b]

Rechargeable batteries currently power much of our world, but with the increased demand for electric vehicles (EVs) capable of traveling hundreds of miles on a single charge, new paradigms are necessary for overcoming the limits of energy density, particularly in rechargeable batteries. The emergence of reversible anionic redox presents a promising direction toward achieving this goal, yet this process has positive and negative effects on battery performance. While it often leads to higher capacity, anionic redox also causes several unfavorable effects like voltage fade, voltage hysteresis, sluggish kinetics, and oxygen loss. However, the introduction of cations with topological chemistry tendencies has created an efficient pathway for achieving long-term oxygen redox with improved kinetics. The cations serve as pillars in the crystal structure and meanwhile can interact with oxygen in ways that affect the oxygen redox process through their impact on the electronic structure. This paper delves into a detailed examination of the fundamental physical and chemical characteristics of oxygen redox and elucidates the crucial role that cations play in this process at the atomic and electronic scales. Furthermore, we present a systematic summary of polycationic systems, with an emphasis on their electrochemical performance, in order to provide perspectives on the development of next-generation cathode materials.

## Introduction

Positioning the future of energy storage, making substantial improvements in the energy density of oxide electrodes becomes increasingly challenging solely through the cationic redox pathway[1-4]. Additional electrons provided by both anionic and cationic redox put one crucial step in overcoming current constraints[5-7]. In addition, the occurrence of concerted anion and cation redox charge compensation, unlike the commercial family of NCM materials with solely cation redox, does not exhibit a great dependence on strategic resources such as cobalt and nickel and presents electrochemical activity in disordered rocksalt structures[8]. This development offers a clear trend towards lowering costs and reducing strategic resource dependence by expanding the choice of cation (normally-believed inert cations) and structure.

Although anionic redox integration with conventional cationic redox-based cathode materials advances ultrahigh energy density and expands the choice of cations, it also poses challenges related to both cation and anion redox[9]. The practical application of anion and cation redox charge compensation in cathode materials is hindered by unfavorable electrochemical properties, including slow kinetics, oxygen loss, voltage fade, and voltage hysteresis. Over the past two decades, researchers have uncovered that these issues stem from oxygen holes stabilized by O-O dimerization and coupled cation migration. Dozens of studies have endeavored different options based on different mechanisms to minimize these challenges.

For instance, examining oxides that can accommodate local structural reorganization produced by O-O dimerization or identifying materials that do not undergo O-O dimerization while simultaneously avoiding transition metal migration and voltage hysteresis.

Indeed, the aforementioned studies on the topic of regulating oxygen redox chemistry always exploit the role of cations, either as mediators of anionic processes, leveraging the fast kinetics and electrochemical stability of cationic redox, or as dopants to control the activation and stabilization of anionic redox through coordination environments. Such nature of oxygen redox along the M-O bond, along with cationic intrinsic pillar roles and electronic structure modification, suggests the pressing need for focusing on the interactions between cation and anion redox. Considering anionic redox chemistry from a cationic perspective is crucial in clarifying the mechanisms behind oxygen redox, ultimately providing opportunities to improve cathode performance and minimize material costs.

In this review, we first examine the physical and chemical properties of oxygen redox as a new redox center different from conventional cationic redox, including its significant benefits and intrinsic challenges. Followed by discussing the action mechanism of cation in regulating oxygen redox. Then, we land on the specific cation selection and the effect of their combination and ordering. Finally, we offer conclusive thoughts on the future of oxygen redox. By exploring the specific roles played by cations in influencing the behavior and performance of oxygen redox, we can gain crucial insights into the design principles and strategies for harnessing the full potential of this intriguing phenomenon.

a. Department of Energy Storage Science and Engineering, School of Metallurgical and Ecological Engineering, University of Science and Technology Beijing, Beijing, 100083 China.
b. Chemical Sciences and Engineering Division, Argonne National Laboratory, Lemont, IL, 60439, USA.
c. Address here.
† Footnotes relating to the title and/or authors should appear here.
Electronic Supplementary Information (ESI) available: [details of any supplementary information available should be included here]. See DOI: 10.1039/x0xx00000x

## 2 The overview of the oxygen redox instincts

Before delving into the topic of the role of cations in oxygen redox, we need to start by understanding the instincts of oxygen redox. Anionic redox is commonly considered synonymous with

ARTICLE

Journal Name

the limit-breaking capacity of cathode materials by providing additional charge compensation. In fact, even when the total deintercalation of alkali is constant, increasing anionic redox increases the capacity per unit of alkali removal. This is because the charge compensation provided by anionic redox is detached from the heavy transition metal. Researchers aim to utilize anionic redox pairs as a complement to low-cost redox electric pairs to increase the additional capacity of cathode materials. However, after the involvement of oxygen redox in charge compensation, several challenges will arise due to the worse reversibility of anion redox and inherent differences in the properties of redox centers between anionic and cationic redox. These challenges include poor capacity retention, sluggish kinetics, voltage decay, and voltage hysteresis. In this section, we will explain the fundamental principles underlying the electrochemical behavior of anion redox, based on the charge-discharge curves of layered oxides that contain typical anion redox. (Fig 1a)

### 2.1 Exceeding the capacity limitation of conventional cathodes

According to Faraday's law, the theoretical specific capacity of rocksalt-structured $Li_{1+x} M^{z+}_{1-x} O_2$ (1>x≥0) materials can be expressed as

$$Q = nZF/M = (1+x)F/[39 + W_M + (7 - W_M)x],$$

Here, Q represents the specific capacity, n signifies the number of ions that can provide electrons, Z is the amount of charge transferred per ion, F is Faraday's constant, and M is the molar mass of the material.

The equation shows that the specific capacity increases with the rise of x, highlighting the need for excess alkali to achieve high capacity. (Fig 1b) However, there is a constraint imposed by the charge balance, which dictates that Z = 1+2/(1-x). This means that as x increases, the valence of the cation is already too high for charge compensation. At this point, oxygen ions can contribute to charge compensation via redox, which enables hyper-lithium oxides to achieve their theoretical capacity, overriding this restriction. Furthermore, achieving high capacity is not only reliant on x but also on the value of $W_M$, the molar mass of the cation. (Fig 1c) Rocksalt-structured oxides are dependent on high-valent transition metals under high excess alkali. Nevertheless, oxygen redox can offer charge compensation without introducing weight gain, enabling the use of lighter but less electrochemically active cations such as $Ti^{4+}$, $Fe^{3+}$, and $Mg^{2+}$. In this way, the use of these lighter, environmentally friendly metals in energy storage is made possible while simultaneously increasing capacity.

Anyhow, the dependence of rocksalt structured oxides on high-valent transition metals under high excess alkali is unavoidable. The extreme utilization of anionic redox capacity entails a departure from rocksalt structures and consideration of structures with an anion-to-cation ratio of less than 1. $Li_2O$ with anti-fluorite structures, for example, solely possesses oxygen redox and has the ultimate theoretical specific capacity. Unfortunately, its poor electrical activity makes it difficult to use. To improve its conductivity, TM doping was utilized to obtain a series of ultra lithium-rich materials such as $Li_5FeO_4$, $Li_6CoO_4$, and $Li_6MnO_4$. $Li_5FeO_4$ can realize the ultra-lithium component with $Fe^{3+}$ and thus obtain high capacity based on simultaneous anion and oxygen ion redox. Ultimately, high capacity as a function of both x and $W_M$, which aligns with anionic redox, indicates that the more anionic redox accounted for, the higher the capacity.
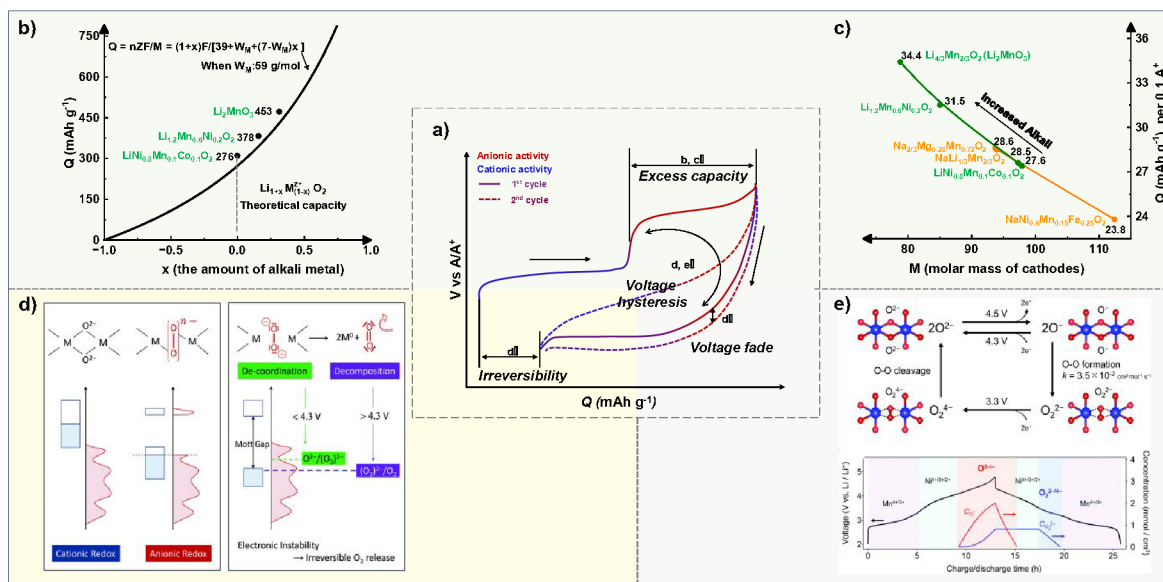


**Figure 1** The instincts of the oxygen redox. a) Typical charge/discharge behavior of layered oxides including anionic redox. b, c) The specific capacity of the cathode material increases as the proportion of anion redox increases, as indicated by the increase in alkali metals and the decrease in molecular mass, as oxygen redox can reduce the reliance on heavy transition metals. c) Schematic of the electrochemical instability of oxidized $O^{2-}$. Reproduced with permission[10]. Copyright Royal Society of Chemistry 2016. d) Kinetic square scheme in O2-$Li_{1.12-y}Ni_{0.17}Mn_{0.71}O_2$, $C(O^-)$ and $C(O_2^{2-})$ as a function of time . Reproduced with permission[11]. Copyright Royal Society of Chemistry 2022.

## 2.2 Limited reversibility triggered by metastable $O^{2-/n-}$ couples

Besides capacity, reversibility and cyclability are the most important metrics for secondary electrode materials. Compared to cationic redox for charge compensation, the drawbacks of anionic redox currently are its poor reversibility and cyclability. For example, researchers have found that irreversible $O_2$ release accounts for 70% of the charging capacity of $Li_2MnO_3$[12]. Furthermore, the cycling performance of cathodes containing oxygen redox is usually inferior to that of cathodes with pure cationic redox. The use of anionic redox is challenging due to the energy loss caused by both voltage hysteresis[13, 14] (150–500 mV during charge and discharge) and voltage decay[15, 16] (300–500 mV after 100 cycles).

The destabilization of anionic redox can be primarily attributed to the characteristics of the desired oxygen redox pair of metastable $O^{2-/n-}$, as shown in equation:

$$O^{2-} \leftrightarrows O^- + e^- \rightarrow 1/2O_2 + 2e^-$$
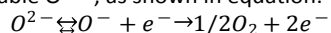
In fact, the redox pair of anionic redox does not exhibit the easy addition or removal of electrons as the conventional transitional metal ions[1]. The loss of electrons in $O^{2-}$ requires higher energy compared to transition metals, as the O 2p bond is located lower than the TM 3d bond. Additionally, as the oxidized $O^{2-}$ potentially are severely underbonded, isolated $O^-$ does not meet the octet rule and is considered unstable, as shown in Fig 1d[17, 18]. This instability leads to phase decomposition into $MO_2$ and $O_2$ during delithiation, which quickly depletes the unhybridized oxygen during charging. The evolution of the $O_2$ is energetically favorable with poor electronic stability of oxidized oxygen, but $O_2$ gas release is irreversible because it leads to the loss of lattice oxygen, thereby rendering capacity unavailable, which needs to be suppressed. Compared to $O_2$ gas, oxidized oxygen in the form of O-O/TM=O bonding is more likely to reversibly regain electrons and return to the $O^{2-}$ state. Doublet et.al.[19] defined that the number of holes produced per oxygen ($h^o$) is an essential parameter in determining the reversible capacity. Therefore, the critical feature associated with reversibility is the stability of the $O^-$ holes.

In sum, the $O^{2-/n-}$ couples are inherently electrochemical instability. The electronic instability of $O^-$ O-holes leads to limited capacity reversibility. The asymmetries between the charging and discharging of $O^{2-/n-}$ redox couples result in poor voltage reversibility. Furthermore, the presence of unstable $O^-$ holes decreases the energy barrier for transition metal (TM) migration, leading to irreversible phase transitions and an increase in low-valent cationic redox, ultimately resulting in electrochemical degradation such as voltage decay. Regulating the stabilizing mechanism of the metastable $O^{2-/n-}$ couples is crucial for the development of reversible oxygen redox.

## 2.3 Power rate associated with the sluggish kinetics

The energy density and power characteristics of electrode materials are crucial indicators for practical applications, particularly in the context of electric vehicles. However, it is commonly observed that capacity contributed by oxygen redox degenerates sharply with the increase of C-rate[20-22], and oxygen redox is accompanied by severe "polarization/overpotential". For instance, the $Li$–$O_2$ battery shows sluggish reaction kinetics and sensitivity to rates[23]. Oxygen reduction and evolution reaction (ORR and OER) in $Li$-$O_2$ batteries require a large overpotential to overcome severe kinetic bottlenecks, which originate from four electron-proton coupled processes and the dismantling of solid products into gas[24, 25]. Likewise, oxygen redox in transition metal oxide cathodes is often regarded as kinetically sluggish. In earlier studies, it was considered that oxygen redox contributes to charge compensation mainly via evolution into O2 gas at a plateau around 4.5V. J. R. Dahn et al. calculated the oxygen diffusion constant in this oxygen loss region of Li-rich oxides to be $10^{-13}$-$10^{-12}$ cm$^2$ s$^{-1}$,[26] which is roughly 1000 times less than the lithium diffusion constant in $LiCoO_2$. When considering reversible oxygen redox, it involves the charge transfer (accepting and donating electrons) process and the accompanying stabilization process. Actually, the kinetics of oxygen redox per se is not slow, while the stabilization process of the $O^-$ along with O-O dimerizations and the motion of TM are the main factors limiting the kinetics. Kosuke proposed the kinetic square scheme to describe the oxygen redox reaction (Fig 1e). During the charging process[11], $O^{2-}$ initially oxidizes to labile $O^-$, and dimerizes to stable peroxide $O_2^{2-}$ with a rate constant of k. During discharge, $O_2^{2-}$ is reduced to the unstable $O_2^{4-}$, then provoking the cleavage to $O^{2-}$. In turn, it has been shown that sluggish local reaction kinetics will trigger electrochemical deterioration of the material, such as cation migration[27].

Besides the electrochemical reaction resistances, chemical diffusivity is also an important parameter affecting the transport rates in solids. Therefore, except for sluggish kinetic processes of oxygen redox, the large voltage gap between charge and discharge in Alkali-rich oxides is additionally ascribed to poor ionic conductivity. In fact, The Li-ion diffusion coefficient in most Li-excess disordered rock-salt oxides ($D_{Li}$: $10^{-16}$–$10^{-15}$ cm$^2$ s$^{-1}$)[28, 29] and layered Li-rich oxides ($D_{Li}$: $10^{-14}$–$10^{-11}$ cm$^2$ s$^{-1}$)[30-32] are far from traditional cathode materials $LiCoO_2$ ($D_{Li}$: $10^{-10}$–$10^{-8}$ cm$^2$ s$^{-1}$)[33]. Therefore, although oxygen redox may be inherently kinetics sluggish, the rate performance of lithium-rich materials can still be improved by increasing the $Li^+$ diffusion coefficient. There are many intriguing studies on acquiring high rate capability in Li-rich materials by facilitating the Li-ion diffusion, such as lattice plane controlling[34, 35], cation doping[36], and nanocrystallization[37], which all demonstrate that involvement of oxygen redox is not an unbreakable limitation on rate capability.

## 3 Concerted cations modulating oxygen redox process

In fact, it is difficult to analyze oxygen redox in isolation within the $AMO_2$ system, as oxygen redox naturally proceeds in concert with cations due to the presence of M-O bonds. Moreover, the additional capacity contributed by oxygen redox may not be fully reversible due to the electrochemical instability of $O^{2-/n-}$ couples. Activation and stabilization are required to enable anionic redox within appropriate potential, providing

high capacity upon prolonged cycling. Actually, the cations, a fundamental component of AMO$_2$, can impact the thermodynamic and kinetic nature of the anion redox, i.e., the TM-O systems can accommodate unstable O and determine its reversibility. It is essential to acknowledge that the electrochemical behavior of oxygen redox is highly correlated with cations, and thus, this section will provide a detailed analysis of the origin and mechanisms of oxygen redox, with a primary focus on the regulation of cations in anion redox processes (O$^{2-/n-}$ couples).

### 3.1 Cations elevate the energy of oxygen 2p state

The capacity of the Li$_{1+x}$ $M_{1-x}^{z+}$ O$_2$ gradually increases as the cation valence rises in the rocksalt structures. For instance, although the capacity of the conventional LiMO$_2$ (M: Ni, Co) system has gradually approached its theoretical capacity and increases yearly, it is still difficult to exceed the limit of 250 mAh/g. In contrast, the Li$_2$MO$_3$ system (M: Mn, Ti, Ru) easily exhibits a capacity of more than 250 mAh/g. Moreover, when further raised to Li$_3$MO$_4$, the layered rocksalt Li$_3$IrO$_4$ can nearly reversibly contribute 356 mAh g$^{-1}$. [38] This is because the Li/TM ratio rises with the increase of cation valence with an anion-to-cation ratio of 1:1 in the rock-salt structures as illustrated in Fig 2a. For example, from LiM$^{3+}$O$_2$, Li$_{4/3}$M$_{2/3}^{4+}$O$_2$, Li$_{3/2}$M$_{1/2}^{5+}$O$_2$ to Li$_{8/5}$M$_{2/5}^{6+}$O$_2$, and the increase in the Li/TM ratio, accompanied by anionic redox involved in charge compensation, can enhance the capacity of the cathode[39], which is the extra capacity provided by anion redox.

However, solely Alkali (A) rich or high valence TM in the rock-salt oxide is not able to guarantee the occurrence of oxygen redox within the working potential window that electrolytes can withstand. The chemical origin of anion redox is the energy increase of the O 2p orbitals. It is because common O 2p hybridized with TM 3d bands along A-O-TM. Therefore, it is commonly proposed that specific cations should be selected to reduce the TM-O hybridization and facilitate the unhybridized O 2p state at the elevated energy level, as shown in Figure 2b. The presence of non-bonding O states raises the energy of the O 2p orbital to induce oxygen redox during deep delithiation[17]. Electrochemically inactive cations, such as alkali, alkali earth, divalent d$^{10}$ transition metals (M), or vacancies(V) with fully filled (or non) d-shells result in weaker and less directional metal-oxygen bonds, favoring the formation of orphaned O 2p states[17, 19].

It was found that the density of states of O 2p non-bonding state is proportional to the number of A-O-A' (M/V) configurations[17] and oxygen redox exhibits a configuration dependence. For example, the cationic charge surrounding one oxygen affects the energy of oxygen non-bonding state in the electronic structure. The lattice oxygen redox was considered be activated in the absence of transition metal (TM)-redoxable species. The generation of the A-O-A' (M/V) configuration can be achieved by decreasing the TM/O ratio. Here, TM refers to ions other than cations favoring the A-O-A' (M/V) configuration.
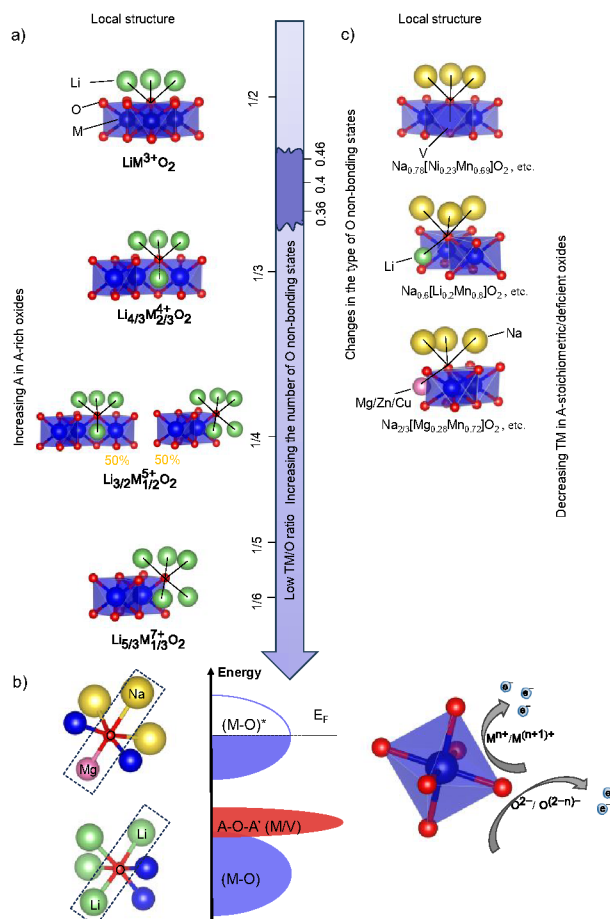


**Figure 2** a) The number of O non-bonding states (A-O-A configuration) in the localized structure increases with decreasing TM/O ratio. a) A-O-A configuration is controlled by cation valence state. Reproduced with permission[40]. Copyright Springer Nature 2018. b) A-O-A configuration reduces the energy level of the oxygen 2p non-bonding orbital, thus leading the oxygen redox. c) A-O-A configuration is controlled by cation specie. Reproduced with permission[41]. Copyright Elsevier 2019.

When A' (M) is A in the A-O-A' (M/V) configuration, a typical lithium-rich or sodium-rich structure is formed. In this case, the cathode theoretical capacity is determined by the number of A-O-A configurations (A/TM ratio). Lithium-rich compounds are the most promising structures for next-generation cathode materials due to the extra capacity of oxygen redox from excess alkali. Sodium-rich compounds also have the potential to offer higher capacity. However, for alkali metal Na$^+$ (1.02 Å) with large radii, it is significantly mismatched with the 3d cation size. Na$_2$MnO$_3$-like materials are only discussed in theoretical calculations[42]. Na-rich oxides are primarily based on Ir/Ru, which struggle to achieve a capacity advantage due to their high molar mass.

When A' (M) is not A in the A-O-A' (M/V) configuration, the participation of oxygen redox does not result in ultimate extra capacity. Therefore, this is more common in sodium-stoichiometric/deficient oxides. Although the substitution of

non-A cations would theoretically sacrifice the ultimate capacity of the material. However, considering the practical de/intercalation of alkali metals, the oxides with non-A cation substitution may not necessarily show a decreased discharge capacity. Furthermore, sodium-based oxides are inherently susceptible to phase transitions during the removal of sodium, Na-rich materials do not exhibit higher capacity and reversibility advantages compared to Na-deficient oxides[43]. In contrast, the reversibility of oxygen redox may be modulated by changing the A'/M/V configuration. Primarily, alkali-rich environments as the conventional paradigm for controlling A-O-A' activation of anion redox, it is also feasible to utilize the Na-O-Li configuration (Fig 2c.) in sodium-ion batteries to activate anionic redox[44] and showed better performance. For example, researchers constructed Na-O-Li bonds by introducing $Li^+$ into the transition metal layer, thereby activating anionic redox in O3-type $NaLi_{1/3}Mn_{2/3}O_2$, which even exhibit improved performance compared to lithium-rich oxides, with little voltage fade during cycling[45]. $Na_xLi_yMn_{(1-y)}$ O2-type oxides are commonly employed in sodium ion cathode materials to activate anion redox. This not only activates higher capacity but also improves cyclic performance by leveraging the pinning effect of $Li^+$ [41, 46, 47]. When x < 1, this suggests that A-deficient oxides can also exhibit anionic redox activity, thereby extending the scenario for the use of anionic redox. Then, divalent activated ions have a stabilizing effect due to stronger electrostatic repulsive interaction. For example, $Mg^{2+}$ as an alkaline earth metal forms an A-O-Mg configuration that possesses labile oxygen electrons due to unhybridized p orbitals[48, 49]. Besides, $Cu^{2+}$ and $Zn^{2+}$ can promote oxygen redox activity through O 2p non-bonding states along with the Cu-O/ Zn-O bond due to the fully localized electrons on the oxygen anion[50, 51]. Therefore, researchers are interested in Na-stoichiometric/deficient oxides that exhibit enhanced reversible anionic redox, which demonstrates high compatibility with anionic redox. Although it is limited by the amount of A content, it is considered a potential candidate for the development of cost-effective energy storage materials, when combined with sodium replenishers.

In summary, the activity of oxygen redox is regulated by cations through the TM/O ratios, thereby further affecting the ratio of anion and cation redox in the system. The theoretical capacity of the system increases as a result of added lighter metals associated with oxygen redox, while the ultimate capacity hinges on the degree of alkali enrichment.

### 3.2 Cation accommodates oxygen redox through hybridization

As mentioned above, the $O^{2-}/O^-$ couple itself is resistant to easy addition or removal of electrons. Therefore, the process of losing electrons of oxygen oxidation involves interactions with cation through hybridization, regulating the activation and stabilization of $O^{2-}/O^-$. The hybridization procedure will determine the electrochemical behavior of anion redox including reversibility and kinetic, which is the origin of asymmetric charging and discharging processes of anion redox and is related to collateral damage such as cation migration.

Before losing electrons of oxygen oxidation, the M-O interaction is actually always present. Although the A-O-A

configuration is able to elevate the energy of oxygen 2p state in the rock-salt oxides as stated before. Compounds such as $Li_2TiO_3$, $Li_2SnO_3$, $Li_2ZrO_3$, and $Li_3NbO_4$, which have abundant A-O-A configurations still fail to exhibit expected oxygen redox activity. This is because in these charge-transfer insulators compounds with either completely empty or completely filled d-shell cations, electrons should be extracted directly from the O non-bonding state. It requires high activation energies and thus induces large overpotentials, pushing the working potential of the oxygen redox over the electrochemical window of the electrolyte.

On contrary, the activation energy can be effectively lowered with the presence of transition metal ions with partially filled d bonds. When M nd-O 2p antibonding states are located at the Fermi energy level, the trigger of oxygen redox can be achieved before the oxidative decomposition of the electrolyte, through the dynamic charge transfer from ligand (O 2p) to metal (M d). Cations can act as intermediate species for oxygen redox[52]. It is shown that transition metal cations with strong M-O covalency have fewer valence electrons in the high oxidation state. This drives the donation of charge from oxygen to the metal center due to low charge transfer energy, which is called LMCT (oxygen oxidation through ligand-to-metal charge transfer)[9]. (Fig 3a) An example of this is the activation process in $Li_2Ir_{1-y}Sn_yO_3$ (LISO) with $Ir^{>5.5+}-O^{2-} \rightarrow Ir^{5.5+}-O^{(2-n)-}$. It was shown that the LMCT process is the beginning of electrochemical irreversibility (anion redox) in $Li_{2-x}Ir_{1-y}Sn_yO_3$, indicating the activation of the LMCT process for anion redox[9]. (Fig 3b) Analogously, since strong d-p hybridization provokes $Ru^{5+}-(O_2)^{2-}$ or $Ru^{4+}-(O_2)^-$ through $Ru^{6+}+O^{2-} \rightarrow Ru^{5+}+O^-$ in $Li_2Ru_{1-y}Sn_yO_3$[53], the oxidation of oxygen may request the TM d orbital to enable the electronic rearrangement of O because electron transfer is afforded by cumulative cations ($M^{n+} \rightarrow M^{(n+1)+}$) and anions ($O^{2-} \rightarrow O_2^{2-}$) through d-p hybridization[54].
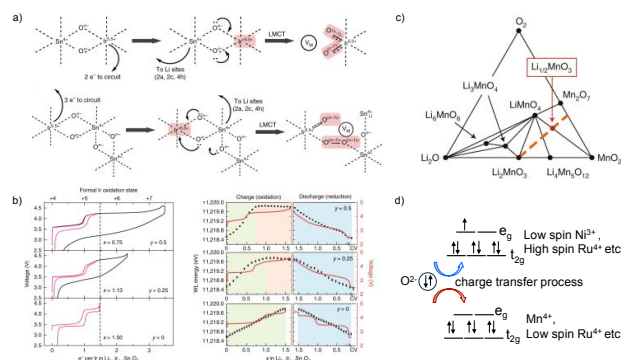


**Figure 3** a) Schematic diagram of mechanisms of anionic redox via ligand-to-metal charge transfer (LMCT) in $Li_2Ir_{1-y}Sn_yO_3$. Reproduced with permission[9]. Copyright Springer Nature 2019. b) The LMCT process is the onset of anion redox. Reproduced with permission[9]. Copyright Springer Nature 2019. c)The metastable phase diagram indicates the oxidation of $Mn^{4+}$ to $Mn^{7+}$. Reproduced with permission[55]. Copyright Springer Nature 2019. d) Charge transfer processes regulate anion redox potentials. Reproduced with permission[56]. Copyright American Chemical Society 2023.

Although first identified in the 4d and 5d transition metals, in fact, this two-step oxidation mechanism also occurs in 3d transition metals[57]. In the case of $Li_2MnO_3$, in contrast to the commonly assumed direct oxygen oxidation mechanism, theoretical calculations have proposed the LMCT process is from O 2p to Mn 3d. When oxygen evolution is kinetically hindered, the oxidation process of $Mn^{4+}$ (oct) to $Mn^{7+}$ (tet) becomes more thermodynamically favorable (Fig 3c), which subsequently triggers the oxygen redox[55]. Recently, researchers have discovered that the LMCT process is universal. This process has been observed in $Ni^{3+/4+}$ and $Co^{4+}$ in Li-rich oxides[58]. Additionally, the LMCT process along with charge redistribution between TM and O[54] will regulate the potential and amount of anion redox[56], (Fig 3d). In conclusion, the LMCT process in the anion redox process is both general and intricate, serving as an approach to facilitate the activation of oxygen redox.

Upon losing electrons, oxygen tends to undergo irreversible redox with the presence of unstable $O^-$ on localized states[59]. Oxidized $O^{2-}$ deviates from the octet rule and tends to form additional covalent bonds for self-stabilization. It was generally considered that the oxidized $O^{2-}$ species can be stabilized by O-O hybridization (also known as O-O dimerization) (Fig 4a), in the formation of dimers in peroxide, superoxide[6, 53, 60], or $O_2$ molecules as trapped in voids[61, 62] (< 1.5 Å), in order to prevent irreversible $O_2$ gas releasing. (Fig 4b) Peroxo-superoxide species can restabilize the oxygen network[45, 53], and trapped $O_2$ molecules[62] within the local environment throughout the bulk can enable reversible oxidation of $O^{2-}$, which both indicate more inclination towards reversible bulk O-redox. However, it has been found that O-O dimerization is accomplished through a multi-step process that involves the migration of the transition metal through an in-plane or out-of-plane to a thermodynamically favorable location to stabilize the distorted oxygen network[63]. At the same time, the emergence of cationic vacancies and dangling oxygen as a result of cation migration in turn promote the formation of O-O dimerization due to the decreased structural rigidity. (Fig 4c) The collateral damage of structural rearrangement of the cation coupled to O-O dimerization will give rise to other issues such as voltage decay due to the correlated irreversible phase transition.
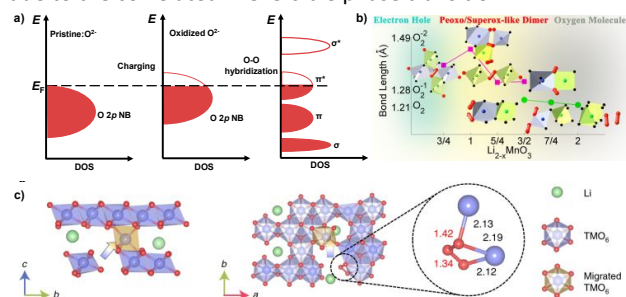


**Figure 4** a) Schematic diagram of the electronic structure of O-O hybridization stabilized $O^-$ holes. Reproduced with permission[64]. Copyright Springer Nature 2022. b) The evolution of O-O dimers involves peroxides, superoxides, and molecular oxygen. Reproduced with permission[65]. Copyright American Chemical Society 2019. c) Transition metal migration coupled to

dangling oxygen involved in O-O dimers. Reproduced with permission[66]. Copyright Springer Nature 2022.

Rather than the O-O hybridization resulting in severe local structure transition, the strong M-O hybridization can stabilize oxidized oxygen through localized π-type interactions with minimal and/or reversible TM migration. Researchers suggest that reversible oxygen redox involves M-O bonds, with σ donation mainly from oxygen before oxidation and π back-donation from M to stabilize oxygen holes after oxidation (Fig 5a). This was proved by the spectroscopic signatures of this π-type hybridization between localized O 2p and M $t_{2g}$ orbitals through RIXS (Fig 5b)[67]. Eum et.al[66] reveals that the large voltage hysteresis of oxygen redox in NLTMO $(Na_{0.6}(Li_{0.2}Ti_{0.2}Mn_{0.6})O_2)$ compared to NLMO $(Na_{0.6}(Li_{0.2}Mn_{0.8})O_2)$ is related to the difference in the oxygen stabilization mechanism. The σ-type cooperative oxygen with O-O dimers replaces π-stabilization between the oxygen and TM by rapid out-of-plane migration in NLTMO, while NLMO exhibits a much slower conversion of π-stabilized oxygen to O-O dimers and thus less voltage decay due to the slow in-plane migration (Fig 5c). Such Metal-Ligand π Interaction is thought to promote reversible oxygen redox in many other cathodes[68-70]. However, further exploration is required to understand the impact of the extent of oxygen network distortion on reversibility, specifically the M-O bond shortening resulting from M-O rehybridization. It has been shown that the TM=O rehybridization may be correlated to reversible cationic migration[64]. Furthermore, it is important to examine the distinction and transformation of π-type cooperative oxygen and O-O dimers.
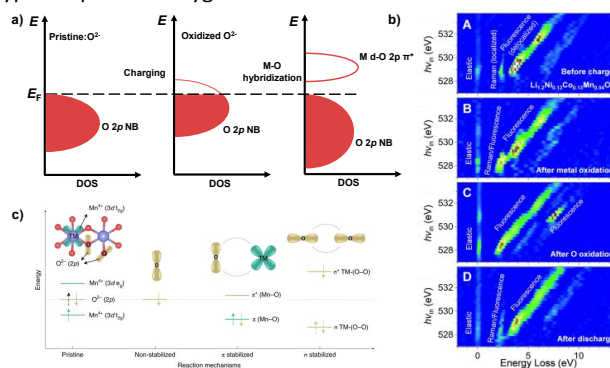


**Figure 5** a) Schematic diagram of the electronic structure of M-O hybridization stabilizes $O^-$ holes. Reproduced with permission[64]. Copyright Springer Nature 2022.b) RIXS spectroscopic evidence of enhanced π-type interactions stabilizes $O^-$ holes. Reproduced with permission[67]. Copyright Royal Society of Chemistry 2020. c) Schematic illustration of the change in stabilizing mechanisms for oxidized oxygen by M-O hybridization and O-O hybridization, respectively. Reproduced with permission[66]. Copyright Springer Nature 2022.

From the above, it can be seen that the reversible oxygen redox is achieved through the M-O rehybridization during the oxygen redox process. (Fig 6a) However, due to the asymmetry of the oxidation and reduction mechanism (Fig 6b), the voltage

         **ARTICLE**

reversibility and kinetics of their electrochemical behavior are limited (Fig 6c). This corresponds to the electrochemical behavior demonstrated by most anion redoxes, such as the typical lithium-rich NCM.
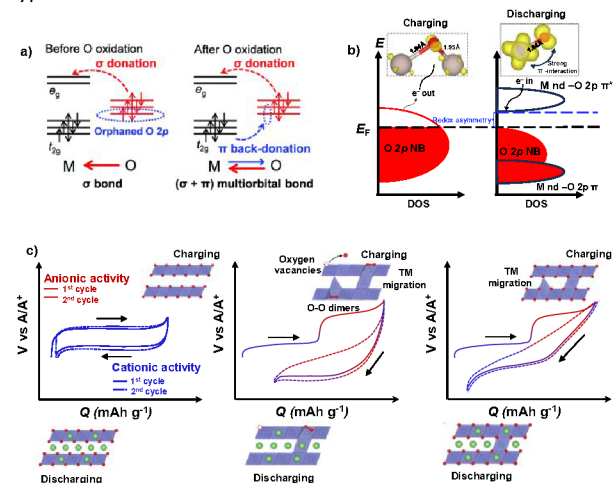


**Figure 6** a) Schematic representation of the stable oxygen redox reaction including σ-accepting and π-donating of metal from oxygen by the M-O rehybridization. Reproduced with permission[67]. Copyright Royal Society of Chemistry 2020. b) Anion redox asymmetry due to the rehybridization mechanism. Reproduced with permission[64]. Copyright Springer Nature 2022. c) Schematic representation of the electrochemical behavior corresponding to different redox mechanisms. Reproduced with permission[64]. Copyright Springer Nature 2022.

As mentioned above, although M-O rehybridization enables reversible oxygen redox, it seems to be correlated with poor voltage reversibility and sluggish kinetics. Hopefully, recent studies have indicated that the electrochemical behavior of $O^{2-}/O^-$ couples (Fig 7a) through delocalized electron holes on (TM-O)$_n$ clusters is relatively more reversible compared to the localized O-O/TM bonding[71, 72]. For example, the researchers proposed that the nonhysteretic extra capacity of $Na_2Mn_3O_7$ originates from the delocalized metal-oxygen π-redox[73]. Specifically, the equivalent Mn-d and O-p orbital contributions to the hybridization can result in the formation of a delocalized large M-O π-bond network, which provides extra capacity. Such a π-system is composed of nonbonded M d-orbital and O-p orbitals within the $M_6$ ring. The π-bond network will generate a novel antibonding state in the band structure, which can serve as the redox center. Such dispersive π-oxygen redox will activate the structure-preserving oxidation and exhibit the excess nonhysteretic capacity by decreasing the free energy as shown in Fig 7a. Furthermore, House related the electrochemical behavior of $Na_{0.6}[Li_{0.2}Mn_{0.8}]O_2$ to the evolution of electron holes on $O^{2-}$, i.e., the transformation from non-hysteretic to large-hysteretic electrochemical behavior, which corresponds to the change from delocalized electron holes to trapped molecular $O_2$ over time. (Fig 7b). Based on comprehensive characterizations, it is generally believed that the mRIXS spectrum of the 527.5eV[71, 74] feature corresponds to

$O^-$ while the 531eV[60] feature and the 523.5eV feature correspond to trapped $O_2$ and O-O dimers.

In conclusion, the oxygen redox processes that do not undergo rehybridization exhibit non-hysteretic electrochemical behavior, regardless of the delocalized electron holes in $Na_{0.6}[Li_{0.2}Mn_{0.8}]O_2$ or the M-O π network in $Na_2Mn_3O_7$[75]. In addition, the non-hysteretic electrochemical behavior also indicates a relatively improvement regarding the sluggish kinetics associated with $O^-$ evolution.[76, 77]. This highlights the significance of modulating the interactions with cations in anionic redox processes.
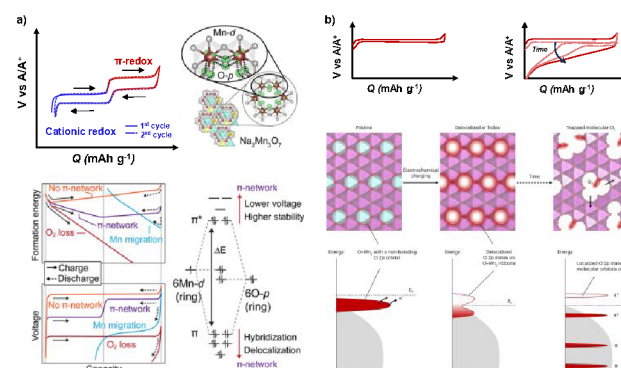


**Figure 7** a) Schematic of excess non-hysteretic anion redox behavior through delocalized M-O π-network and schematic of the free energy and energy level diagram for π-redox. Reproduced with permission[73]. Copyright American Chemical Society 2021. b) The conversion of delocalized oxygen to the O-O dimer over time corresponds to a transition from non-hysteretic oxygen redox to hysteretic electrochemical behavior and the schematic representation of delocalized electron-hole on oxygen evolving into an O-O dimer over time. Reproduced with permission[71]. Copyright Springer Nature 2023.

### 3.3 Pillar cations to ensure topochemistry of oxygen redox

In a typical cathode material based mainly on cationic redox, the secondary cathodic behavior is achieved by topological chemical reactions that maintain the crystal structure during the insertion and abstraction of Li ions, with only lattice expansion occurring in the perpendicular direction[78]. For instance, in the layered oxide $LiNi_xMn_yCo_zO_2$ cathode (NMC), the electrochemically inert metal ions such as $Mn^{4+}$ are often used to improve structural rigidity and act as the reaction framework for topological chemistry to enhance ion transport channels. Likewise, anionic redox also required the stability of the layered structure to ensure the topochemical charge-discharge properties. As mentioned above, however, structural rearrangement and transition metal migration($O^{2-} + TM \rightarrow O^- + TM_{mig} + e^-$)[66, 79] are deeply coupled with the oxygen redox for the stabilization of the band structure, which helps to prevent irreversible oxygen gas release but adversely impacts the local ordering of materials[64].

The electrochemical degradation induced by the irreversible cation migration accompanying the anionic redox process emphasizes the importance of the structural integrity of interlayer/

intralayer cations. Researchers have correlated heterogeneous structural dynamics of LiTMO$_2$ and Li$_2$MnO$_3$ nanodomains with electrochemical degradation in lithium-rich oxides[27]. The lattice strain due to the heterogeneous structure and reaction kinetics will provoke TM migration[80]. (Fig 8a) Conversely, anionic redox can also be stabilized by improving the structural integrity of cation layers. Yamada explains the better reversibility of Na$_2$RuO$_3$ due to the self-repairing layer stacking triggered by robust pillars of remaining A ions[81]. Recently, it was found that P3-Na$_{0.6}$Li$_{0.2}$Mn$_{0.8}$O$_2$ with the -α-γ-layer stacking can preserve the reversibility of lattice oxygen redox through topological protection[82]. Eum found that the local structure of face-sharing between TMO$_6$ octahedra and LiO$_6$ octahedra exhibits more reversible anionic redox. This is due to the strong electrostatic repulsion between cations, which hinders the TM migration compared to edge-sharing[83, 84]. Liu et al. demonstrated that by placing transition metal (TM) ions as a "cap" above or below lithium (Li) ions to anchor the honeycomb structure, the reversible lattice oxygen redox of Li$_{1.1}$(Ni$_{0.21}$Mn$_{0.65}$Al$_{0.04}$)O$_2$ with negligible voltage decay can be achieved[85].

Therefore, in anionic redox systems, higher structural stability is required to stabilize the oxygen network. Specific cations can benefit structural integrity, thus enhancing anion redox cyclability and is highly resistant to voltage decay. Cationic doping is widely applied and the key indicator of the substitution element to improve the oxygen redox electrochemical performance is the degree of disorder (A/TM mixing), which is also a fundamental factor affecting the stability of the structure[86]. Alkali/alkali earth metals in the transition metal layer also stabilize the oxygen redox through structural factors. For example, the larger cations (Na$^+$, K$^+$) doping in the alkali site can suppress cation migration at the charged state through the pinning effect [87, 88], and the divalent cations (Mg$^{2+}$ and Zn$^{2+}$) prefer to be retained in original octahedral sites due to electrostatic effects thus reducing mobility[89]. In addition, adjusting the ratio of cationic redox to anionic redox also results in a more reversible electrochemical behavior of oxygen redox due to the structural stabilization network of cationic redox. Li-rich systems with raised nickel content can achieve both high energy and long cycles with reversible capacity above 250 mAh/g and capacity retention above 90% after hundreds of cycles[90, 91]. The lifetime of pure anionic redox cathodes does not exceed 50 cycles, while mixed anion and cation cathodes will exceed 300 cycles.

Furthermore, cationic intralayer/interlayer arrangement and interlayer stacking are also crucial for structural integrity. Therefore, the sodium-ion system may exhibit better maintenance of structural integrity with homogeneous oxygen redox compared to the lithium-ion system. Tarascon suggested that P2-type stacking is more suitable as a framework for stabilizing oxygen redox, allowing for homogeneous oxygen oxidation and maintaining interlayer O-O bonds, while O2 stacking tends to lead to a disproportionation of the oxygen network[92]. (Fig 8b) In addition, Chen et al. proposed that the P3-type structure restricts the out-of-plane migration of transition metals due to the size mismatch between the TM ions and Na sites and provides space to hold O-O dimerization[93].

In sum, the stability of anionic redox is closely correlated with the reaction framework of the topological chemistry of cations. Stable oxygen networks that can accommodate reversible anion redox are crucial, which can be achieved by tuning the chemical and structural rigidity, cationic intralayer/interlayer arrangement, and interlayer stacking.
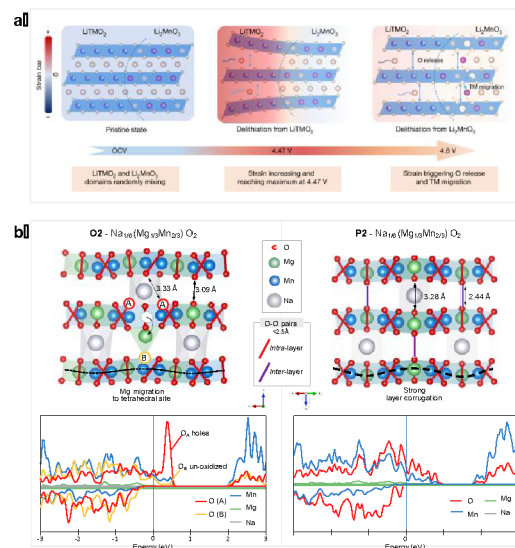


**Figure 8** a) Heterogeneous nanostrain of LiTMO$_2$ and Li$_2$MnO$_3$ domains triggers oxygen release and TM migration. Reproduced with permission[80]. Copyright Springer Nature 2022. b) P2-type stacking is more suitable as a framework for stabilizing oxygen redox, allowing for homogeneous oxygen oxidation and maintaining interlayer O-O bonding. Reproduced with permission[92]. Copyright Elsevier 2020.

## 4 Building an appropriate "transition metal" (A$_x$M$_{1-x}$O$_2$) slab for oxygen redox with high capacity and long cycle life

The geometrical and electronic structures of cations play a crucial role in affecting the kinetics and thermodynamics of oxygen redox, as discussed above. Cations with varying valence, size, electronegativity, and TM-O binding energy exert physical and chemical interactions that impact the activation and stabilization of oxygen redox. Hence, creating an appropriate A$_x$M$_{1-x}$O$_2$ slab presents the potential for oxygen redox to offer higher capacity with improved reversibility, serving as an additional charge compensator to aid in cathode material advancement.

This section will explain the construction of an A$_x$M$_{1-x}$O$_2$ slab capable of accommodating oxygen redox. The first step involves carefully selecting specific cations to be included in the M layer based on their physicochemical properties (Fig. 9a). In addition, it is important to note that in anionic redox systems, there is a selective increase in the availability of cations due to reduced dependence on the electrochemical activity of the cations. Therefore, more consideration should be given to the earth's abundance and price of cations. Figure 9b, c the geophysical abundance and cost of common cations in cathode materials,

　　　　　　　　　　　　　　　　　　　　　　　　　　　　　　　　　　　　　**ARTICLE**

respectively. Following cation selection, it is equally important to consider the combined and ordering effects of multiple cations in the M layer on oxygen redox.
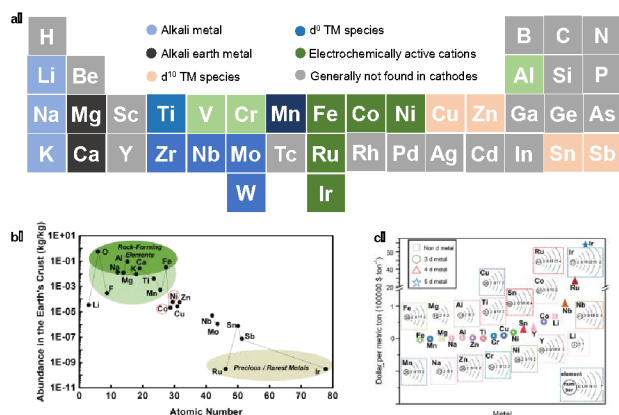


**Figure 9** a) Index several common types of transition metals in cathodes through the periodic table of elements. b) Abundance in the Earth's crust of common metals in cathodes. Reproduced with permission[94]. Copyright Royal Society of Chemistry 2011. c) Prices in $ per metric ton of TMs commonly used in cathodes. Reproduced with permission[95]. Copyright John Wiley and Sons 2021.

### 4.1 Selection of appropriate cations

In an anion redox system, the primary role of cations is to activate and stabilize anionic redox while also accommodating excess alkali metals and providing stable capacity themselves ideally. However, a single cation cannot fulfill all roles simultaneously; at the same time, a single cation may assume multiple roles. The selection of the appropriate cation is intricate. Generally, cations with similar physicochemical properties have comparable effects on oxygen redox, although specific outcomes may still differ. We will discuss the desired roles of cations from the perspective of their physicochemical properties. Among them, the stabilizing role of complexity and diversity will be discussed in relation to other roles. This understanding is essential for designing materials to achieve high capacity and reversibility with both anion and cation redox.

First, in order to activate oxygen redox for charge compensation, the presence of higher-energy unhybridized O 2p states is necessary. This requirement calls for the existence of cations with weaker and less directional metal-oxygen bonds in the M-layer, such as alkali and alkaline earth metals, and divalent $d^{10}$ metals. Among them, $Li^+$ is the most commonly used cation due to its lighter molar mass, which inherently increases the theoretical specific capacity of the system. Then, cations with relatively heavier molar mass, such as $Na^+$, $Mg^{2+}$, $Cu^{2+}$, and $Zn^{2+}$, may exhibit a less pronounced capacity-enhancing effect compared to $Li^+$. However, they are capable of enhancing reversibility. For example, $Mg^{2+}$ remains in the lattice thereby stabilizing lattice oxygen through stronger electrostatic repulsive interaction[48, 96, 97]. Moreover, $Cu^{2+}$ and $Zn^{2+}$ contribute to increased rigidity of the oxygen framework, consequently enhancing the reversibility of the oxygen redox[98].

Secondly, in order to enable the provision of ultimate capacity through anionic redox, the alkali-rich structure is preferred over the alkali-stoichiometric. High valence cations are the fundamental components of alkali-rich anionic redox systems, common $A_{1+x}MO_{2+x}$ systems consist of high-valence cations including $Mn^{4+}$, $d^0$ metals[99, 100] such as $Ti^{4+}$/ $Mo^{6+}$/ $Nb^{5+}$, $d^{10}$ metal ions like $Sn^{4+}$/$Sb^{5+}$, and highly covalent 4d/5d metals of $Ru^{4+}$/$Ir^{4+}$. Among them, the highly valent cations encompass strong covalent cations ($Ru^{4+}$, $Ir^{4+}$), which are viewed as exemplifying the reversible anionic redox process through the charge compensation involving mixed cations ($M^{n+} \rightarrow M^{(n+1)+}$) and anions ($O^{2-} \rightarrow O_2^{2-}$), facilitated by the strong M-O bond[64]. However, the utilization of 4d and 5d metals is limited due to their scarcity and heavy mass. In addition, the $Ru^{4+}$ and $Ir^{4+}$ remain electrochemically active at high valency and can achieve charge compensation by cationic redox with high alkali contents, requiring particular caution when exploring anionic redox. For example, the primary contributor to the capacity of $Li_2IrO_3$ materials has been shown to originate from the $Ir^{4+}/Ir^{5.5+}$ redox couple, whose reversible electrochemical behavior cannot explain the fundamental principles of anion redox. In contrast, cations with $d^0$ ($Zr^{4+}$, $Nb^{5+}$, $W^{5+}$, $Ta^{5+}$) and $d^{10}$ ($Sn^{4+}$, $Sb^{5+}$, and $Te^{6+}$) electronic configurations have relatively ionic TM-O bonds, resulting in them as charge transfer insulators. These inactive cations can enhance the hole localization of the oxide ions and spontaneous metal–oxygen decoordination upon oxygen oxidation[19, 64], resulting in the presence of dangling oxygen[101, 102]. This promotes the formation of localized O-O single bond[36, 103]. (Fig 10 a-c) While the special inert $Ti^{4+}$ ($3d$-$t_{2g}^0$ $e_g^0$) are relatively inactive in oxygen redox reactions[104]. Theoretical calculations indicate that the $O^{2-}/O^{n-}$ redox reaction potentials in $Li_2TiO_3$ are as high as approximately 4.86 V vs $Li/Li^+$, which exceeds the voltage window of the electrolyte[105, 106]. Therefore, the rigid structure of the non-bonding O-TM state and no electrons available in the valence band in the electron configuration can serve as a "potential-pillar" to stabilize structures[107, 108]. $Ti^{4+}$ cation tends to effectively maintain electrostatic repulsion of the lattice $O^{2-}$ in the M-layer due to the nonreactive nature during the voltage window[108-110], leading to the stabilization of oxygen redox. With the raising of inactive $Ti^{4+}$ (not available for charge compensation), $Li_{1.2}Ti_{0.6}Mn_{0.2}O_2$ instead of $Li_{1.2}Ti_{0.4}Mn_{0.4}O_2$) exhibits higher capacity and better cycle performance due to the strengthened networks of strong electrostatic repulsion[108, 111]. Compared to the aforementioned cations, the $Mn^{4+}$ with 3 d-$t_{2g}^3$ electronic configuration exhibits both electron acceptance and donation abilities, making it highly compatible with anionic redox and perhaps a more appropriate choice. For example, It has been shown that $Mn^{4+}$ with the relatively ionic ($Mn^{4+}/Li^+$)-O interaction can promote the localization of electron holes on oxygen[112] and it has also been reported that stable $Mn^{4+}$-O−• coupling is the origin of reversible nonhysteretic oxygen redox[113]. As a result, Mn-based oxygen redox systems such as $Li_2MnO_3$[114-116], $Na_{0.6}[Li_{0.2}Mn_{0.8}]O_2$, and $Na_2Mn_3O_7$[75] have attracted extensive research in the battery industry. In the end, it needs to be mentioned that with cycling the valence state of the high valence cations decreases and the proportion involved

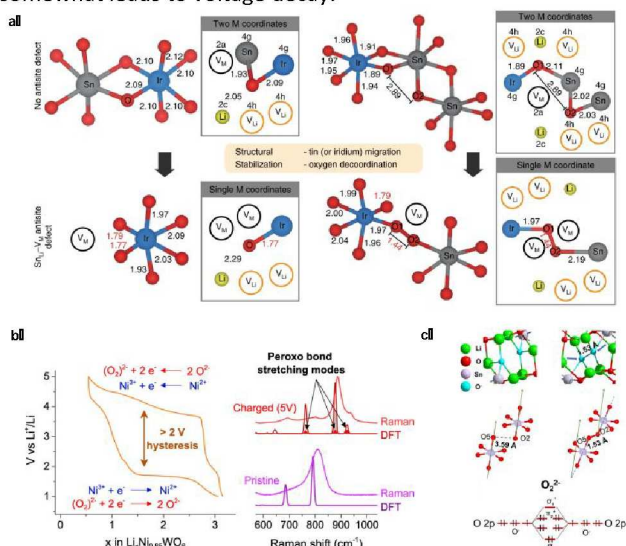in charge compensation gradually increases[117], which somewhat leads to voltage decay.



**Figure 10** The role of high-valent cations. a) M-O decoordination promotes the formation of O-O dimer to stabilize O holes. Reproduced with permission[9]. Copyright Springer Nature 2019. b) Stabilization of peroxo bonds by d[0] Cations(W[5+]). Reproduced with permission[103]. Copyright American Chemical Society 2019. c) $Li_8SnO_6$ to $Li_6SnO_6$ with the formation of O–O dimers. Reproduced with permission[101]. Copyright American Chemical Society 2021.

Thirdly, the low-valence active cations are used in anion redox systems due to their own stable and large capacity. These low-valent 3d metal cations like $Fe^{3+}$, $Co^{3+}$, and $Ni^{2+}$ undergo simultaneous or asynchronous cationic redox with oxygen redox. As a result, the combined cationic and anionic redox offers advantages in reversibility, cyclability, and high capacity. Moreover, the active cations have a significant but not identical impact on anionic redox through the covalent M-O bonds. Fig 11a-c illustrates the quantitative electron shell energy relationship between the bands of these TM redox pairs and the O 2p band according to the electrochemical behavior of $NaMO_2$. Put simply, the degree of coupling between the cationic and anionic redox reactions varies depending on the energy differences between the O 2p band and the $M^{3+/4+}$ band. Firstly, as an environmentally friendly earth-abundant element, Fe has attracted much attention for its role in anion redox. $Fe^{3+}$, with its d5 configuration, exhibits a pronounced $Fe^{4+} \rightarrow Fe^{3+}$ process that affects anionic redox. Researchers explored that $Li_5FeO_4$ could achieve simultaneous and reversible cationic and anionic redox between $Li_3FeO_{3.5}$ and $Li_4FeO_{3.5}$[118]. (Fig 11d) $Fe^{3+}$ can also stabilize oxygen redox and show better cycling performance, due to the formation of Fe-(O-O) species[119-121]. (Fig 11e) $Co^{3+/4+}$ redox centers exhibit fast electrochemical kinetics and small energy differences with O 2p, facilitating the kinetics and thermodynamics of anionic redox. It has been observed that rapid $Co^{3+/4+}$ can promote oxygen kinetics due to the strong hybridization of TM-d and O-2p orbitals during the oxygen redox process. Li et al. demonstrated this phenomenon in their

study, where perfect overlap of $Li_{1.2}Ru_{0.4}Co_{0.4}O_2$ above 3.7 V with increasing C rate in dQ/dV profiles indicated that $Co^{3+/(3+\delta)+}$ with more facile kinetics can expedite oxygen redox through tough coupling, thereby acting as an oxygen redox mediator[122] (Fig 11f). Additionally, $Co^{3+/(3+\delta)+}$ with fast kinetics was found to elevate transport pathways in $Li_2O$ as a skeleton[123] (Fig 11g). Overall, the fast electrochemical kinetics and small energy difference of $Co^{3+/4+}$ with O 2p contribute to the enhanced dynamic and activation of anionic redox. $Ni^{2+}$ is the major electron-donating cation and has a long-term stable cationic redox capacity. So increasing Ni content can alter the redox center and positively affect the thermodynamics and kinetics of oxygen redox through the shielding effect[91, 124-126]. (Fig 11h) In addition, it has been demonstrated that $Ni^{3+/4+}$ is less effective than Fe/Co in activating anionic redox, and relatively more beneficial in stabilizing the structure[120, 127]. Therefore, "Lithium-rich nickel-rich" oxide is a popular strategy for trading off high capacity and reversibility[128].

Additionally, this suggests that traditional layered materials (such as Ni-rich layered oxides >4.3 V[129] and $LiCoO_2$ >4.2 V[130-132]) often involve oxygen redox, commonly known as oxygen loss, at higher states of charge[132-134].

$$LiM^{3+}O_2 \leftrightarrow Li_{(1-x)}M^{>3+}O_2^{>2-} + xLi^+ + xe \ (1 \geq x > 0)$$
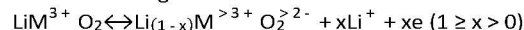
According to the reaction, we can know that when TM is not in the fully oxidized state, the involvement of oxygen in charge exchange merely modifies the redox center instead of contributing to de-lithiation. However, the strong hybridization of the M-O bond, resulting from the overlap of M 3d and top O 2p orbitals, enables both TM cations and lattice oxygen to be involved in charge compensation through TM-O rehybridization during deep delithiation[135, 136]. The $Co^{3+/4+}$ couple exhibits earlier oxygen redox due to the overlap between $Co^{3+}$ t2g orbitals and O 2p orbitals[137, 138], while the $Ni^{3+/4+}$ couple undergoes oxygen redox at deeper delithiation[139]. This is similar to the described role of $Ni^{3+/4+}$ and $Co^{4+}$ as intermediates in triggering anion redox through LMCT in Li-rich NCM[58]. It can be seen that the participation of oxygen redox does not always result in extra capacity, but in transition metal oxides, achieving higher capacity may inevitably involve oxygen redox.
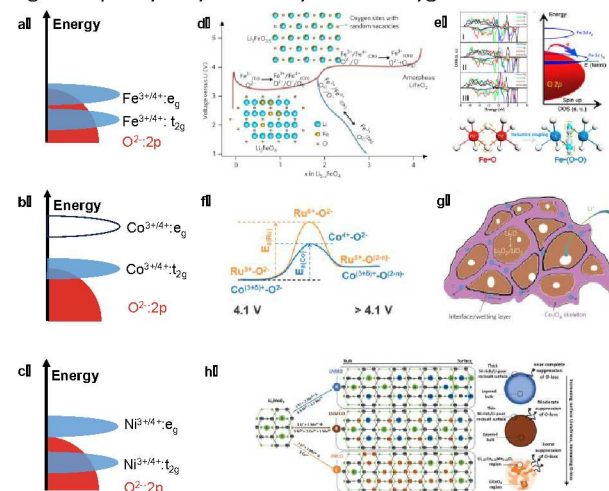
ARTICLE

**Figure 11** The role of 3d metal Fe/Co/Ni. a, b, c) Schematic representation of the relative energy of the $Fe^{3+/4+}$/ $Co^{3+/4+}$ / $Ni^{3+/4+}$ band and the O 2p band, respectively d) Simultaneous $Fe^{3+/4+}$ and $O^{2-/-}$ were observed in $Li_5FeO_4$. Reproduced with permission[118]. Copyright Springer Nature 2017. e) Fe stabilizes oxygen by forming Fe-(O-O) species by the reductive coupling mechanism. Reproduced with permission[121]. Copyright American Chemical Society 2020. f) Schematic of the effect of activation energy (Ea) in different cationic intermediate states on oxygen kinetics. Reproduced with permission[122]. Copyright American Chemical Society 2020. g) Schematic of the $Co_3O_4$ skeleton as a diffusion channel for lithium ions in $Li_2O/Li_2O_2/LiO_2$. Reproduced with permission[123]. Copyright Springer Nature 2016. h) Ni contributes to the maintenance of the structure and thus exhibits a more reversible oxygen redox. Reproduced with permission[124]. Copyright John Wiley and Sons 2020.

#### 4.2 Considering the combinations and ordering of multi cations

Multiple cationic complexes will have multi-level effects on anion redox compared to single cations, synergistically enhancing each other, or inherently limiting TM migration through ordering. By adjusting the combinations and ordering of multiple cations, it is possible to alleviate the limitations of current oxygen redox and achieve long-term reversible and high-capacity oxygen redox.

First, when examining capacity, cycle life, and kinetic properties, using a combination of multiple cations as a framework for anion redox is more suitable than relying on a single cation due to the multiple roles required to regulate anion redox. On the one hand, typical anionic redox systems always contain high valence cations to increase alkali-rich environments and electrochemically active cations to enhance reversibility and kinetics. For example, cubic $Li_2TiO_3$ is not electrochemically active; however, the introduction of active cations triggers substantial oxygen redox[140, 141], leading to a reversible capacity of 250 mAh g$^{-1}$ in $Li_{1.2}Ti_{0.4}Fe_{0.4}O_2$[140]. Besides, the combination of cations with different chemical properties will induce different redox activity. For example, $Li_{1.2}Ni_{0.2}M_{0.6}O_2$ (M: Mn/Ru) (LNMO / LNRO) with similar crystal structures exhibit approximate capacity but completely different electrochemical behavior[142], with active oxygen redox in LNMO and active cation redox in LNRO. Likewise, the electrochemical behavior of anion redox exhibits complex and multifaceted changes with the same $Mn^{4+}$ and different A' combinations. It has been found that $Na_{0.6}[Li_{0.2}Mn_{0.8}]O_2$ and $Na_{2/3}[Mg_{1/3}Mn_{2/3}]O_2$ electrode materials, both with the sole and substantial oxygen redox activity, yet exhibit entirely distinct lattice oxygen redox behavior[60, 143]. $Na_{2/3}[Mg_{1/3}Mn_{2/3}]O_2$ activates higher anionic redox capacity and demonstrates good long-term cyclability but large voltage hysteresis, while $Na_{0.6}[Li_{0.2}Mn_{0.8}]O_2$ displays ultra-high first-cycle coulomb efficiency and good voltage reversibility but few cyclability. On the other hand, studies have shown that there are synergistic effects resulting from multiple cation coordination. Significant progress has been made through the use of element substitutions and blending doping elements (<1%). Similarly, high-entropy systems (> 5 elements) that combine the advantages of a wide range of cations have

captured the attention of researchers due to the extended cycle life of cathodes. However, further exploration is needed to understand the effect of the coexistence of multiple cations on anion redox, either in a simple parallel manner or through coupled interactions[144, 145]. Overall, optimizing the capacity and reversibility of anionic redox systems can be achieved by rational design of cation composition and content.

Moreover, the cations in the TM layer are not randomly distributed. For example, in order to minimize the electrostatic energy, the high-valent $Mn^{4+}$ will be orderly distributed around the low-valent $Li^+$ ($LiMn_6$), leading to the so-called honeycomb superstructure[146]. Influenced by charge ordering, the introduction of low-valence transition metals promotes honeycomb ordering. For instance, the divalent ion $Ni^{2+}$ is capable of maintaining the honeycomb ordering through two competing charge orderings: $Ni^{2+}-Mn^{4+}$ and $Li^+-Mn^{4+}$. Likewise, $Fe^{3+}$ has been proposed to tend to honeycomb structure formation[147]. Although trivalent ions may have a weaker impact compared to divalent ions, it has been demonstrated that $Co^{3+}$ reduces the electrostatic energy of $Li^+-Mn_6^{4+}$ ordering by in-plane geometrical frustration[148]. The superstructure can seriously affect the cycle life of the material, it has been shown that even for the same elemental species, different ratios will significantly affect the electrochemical behavior. This is the impact of the control of cation ordering. Along with the variation of cation ratios, the local arrangement will significantly change. For example, the researchers found that given electrostatic interactions between high-valence cations and low-valence cations, the atomic ratio of ($Mn^{4+}$ and $Co^{3+}$) and ($Li^+$ and $Ni^{2+}$)=2:1 in the transition metal layer favors the formation of a perfect Honeycomb superstructure, which can accommodate oxygen redox while preserving the layered structure[149]. (Fig 12a) The local arrangement with different cation ordering is inherently different in structural stability. Bruce observed the presence of -Li-4Mn-Li- sequences in $Na_{0.6}[Li_{0.2}Mn_{0.8}]O_2$, which exhibit Ribbon superstructures that inhibit TM in-plane migration and suppress voltage hysteresis compared to the conventional honeycomb structure in $Na_{0.75}[Li_{0.25}Mn_{0.75}]O_2$[150]. (Fig 12b) Similarly, $Li_{1.1}(Ni_{0.21}Mn_{0.65}Al_{0.04})O_2$ with a capped-honeycomb superstructure can exhibit electrochemical behavior with negligible voltage hysteresis, and it also suppresses oxygen release, cation migration, and phase transitions[85]. (Fig 12c) The stabilization of superstructure motifs has been widely used to suppress oxygen loss in cathodes with anion redox. For instance, $Mn_6Mg$ ordering is employed instead of $Mn_6Li$ ordering[97], and "entropic stabilization effects" are also utilized[144].
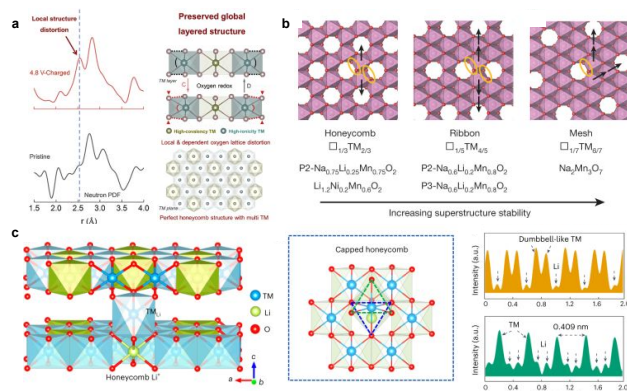
**Figure 12** a) Schematic for TM coordinate distorted oxygen lattice. Reproduced with permission[149]. Copyright Elsevier 2020. b) Schematic of the cation migration paths in different local superstructure. Reproduced with permission[150]. Copyright Springer Nature 2019. c) The capped-honeycomb structure inhibits the migration of transition metals, resulting in improved reversibility of anionic redox. Reproduced with permission[85]. Copyright Springer Nature 2023.

Then, without requiring specific cation ordering, disordered rock-salt structures (DRX) have attracted attention with structure-induced anionic redox activity and broader cation options. DRX was initially believed to be limited in lithium diffusion due to the reduction of the Li slab spacing. Subsequently, Ceder points out that the 0-TM percolation network (without octahedral transition metals) is active when enough Li excess is introduced,[151] which sets on a new path to develop oxygen redox, especially for the structural altering oxygen redox. For example, it was found that electrodes with cations partially disordered can suppress voltage fading better than cations well-ordered[152]. Cation migration even spurs novel opportunities in power density in cation-disordered materials. Ju Li et al. proposed that oxygen-redox-coupled structural reorganizations may disrupt medium-range-order in Li-rich layered materials, which are beneficial to kinetics[153]. Ceder and coworkers suggest that fast and reversible oct-tet cation migration is promising for fast Li transport in Li-rich disordered-rocksalt oxides[29]. Although such compounds also exhibit rapid capacity and voltage decay[141], which stems from high capacity-dependent oxygen redox and low TM redox caused by the excessive Li and low TM for increasing percolating Li. DRX is still an effective path for the development of anionic redox. Fluorinated DRXs facilitate cation over stoichiometry to mitigate the issue of low TM redox. Ceder introduces a high-capacity $Mn^{2+/4+}$ double redox coupled with a small voltage fade by replacing $O^{2-}$ with low-valent $F^{-}$[154]. Fluorination is a prominent direction for developing DRXs materials due to its compatibility with higher lithiation and more reversible capacities[155, 156]. Furthermore, Li-rich disordered rocksalt (DRX) materials offer an important direction for improving the rate capability of Li-rich oxides. Cho's group revealed the significant difference of Li-rich cation-ordered/disordered oxides at high C-rates when discharging <3.5 V and interpreted it as the deviation between the surface and bulk[157]. Ceder et al. found

short-range order (SRO) of the cations in DRX, which will affect local arrangement and thus exhibit unique lithium transport characteristics[158], and showed high-entropy cathodes can deliver 170 mAh g$^{-1}$ at a high discharge rate of 2,000 mA g$^{-1}$ with SRO disruption[159]. Therefore, the DRX oxides bring new dynamics to the development of anionic redox.

## Conclusions

Generally, anionic and cationic redox each offer distinct advantages for charge compensation. The unique topological chemistry of the cationic tendency in the electrode material enhances reversibility, while the participation of anions in charge compensation has the potential to address energy limitations, albeit with highly metastable processes that can lead to irreversible damage. Consequently, achieving long-term reversible oxygen redox requires attention to the complex interaction between cations and anions. We summarize the cationic action mechanism based on the TM/O ratio, M-O hybridization, and reaction framework. The complex interaction between cations and anions drives oxygen redox in different ways, leading to diverse properties. However, the cationic action mechanism in anion redox processes may be more complex than currently proposed. Focusing on the coupling between anions and cations and further exploring this relationship can help achieve a balance between system reversibility and the involvement of oxygen in charge compensation.

Among them, cation migration, which can stabilize oxygen holes, is a significant degradation mechanism that impacts reversibility and stability. Despite studies increasingly showing the emergence of active O$^-$ without cation migrations, none of them are stable in the long term. The suppression of irreversible cation migration in long-term cycles continues to be an inescapable challenge for the development of reversible anion redox. Multi-cation compound oxides that incorporate various combinations and ordering have proven to be superior to perturbed migration in addressing this issue. It is worth noting that the effect of adding cations is multiscale. Further exploration of different electrochemical activities, ratios, and valence states of cations, along with a consideration of structural and chemical modifications, will enable the discovery of more advanced cathode materials. It is possible to maintain the reversibility of the oxygen redox while utilizing numerous cationic redox in a multi-cationic system, providing potential opportunities for the future advancement of oxygen redox. a deterioration mechanism exists where cation migration stabilizes oxygen redox.

The battery industry constantly requires cathode materials to increase energy density, which can be achieved through the utilization of high-valent cationic redox and anionic redox. Oxygen redox has gained significant attention as a supplement to current transition metal-redox couples, owing to its presence in many systems that strive for higher energies. It seems an inevitable aspect of the advancement of high-capacity layered transition metal oxide cathode materials. It is important to note that the advantages and disadvantages of anionic redox vary

across different systems. For example, the high occurrence of non-hysteresis anion redox in $Na_{4/7-x}(1/7Mn_{6/7})O_2$[160], $Na_2Mn_3O_7$[75, 161], and $Na_{0.6}[Li_{0.2}Mn_{0.8}]O_2$[150] et al. highlights the strong compatibility of the sodium ion system with anionic redox. It provides a promising direction for achieving anionic redox with long-period stability and fast kinetics. However, additional capacity still needs to be realized through A-rich, and Li-rich materials are the most promising components for breaking through the energy density of cathode materials. The development of anionic redox systems that are abundant in earth elements, and that take into account both high capacity and reversibility by controlling the structure and reducing the lithium-rich content, remains an important focus. In the case of conventional transition metal oxides for anionic redox coupled with cationic redox, it can be further integrated with the experience of mature lithium-rich material systems to maintain reversibility close to the theoretical capacity.

## Conflicts of interest

There are no conflicts to declare.

## Acknowledgements

## Notes and references

1.      M. S. Whittingham, *Chemical reviews*, 2004, **104**, 4271-4302.
2.      S.-K. Jung and K. Kang, *Nature Energy*, 2017, **2**, 912-913.
3.      K. A. Jarvis, Z. Deng, L. F. Allard, A. Manthiram and P. J. Ferreira, *Chemistry of materials*, 2011, **23**, 3614-3621.
4.      S. Hy, H. Liu, M. Zhang, D. Qian, B.-J. Hwang and Y. S. Meng, *Energy & Environmental Science*, 2016, **9**, 1931-1954.
5.      K. Luo, M. R. Roberts, R. Hao, N. Guerrini, D. M. Pickup, Y.-S. Liu, K. Edström, J. Guo, A. V. Chadwick and L. C. Duda, *Nature chemistry*, 2016, **8**, 684.
6.      E. McCalla, A. M. Abakumov, M. Saubanère, D. Foix, E. J. Berg, G. Rousse, M.-L. Doublet, D. Gonbeau, P. Novák and G. Van Tendeloo, *Science*, 2015, **350**, 1516-1521.
7.      M. Li, T. Liu, X. Bi, Z. Chen, K. Amine, C. Zhong and J. Lu, *Chemical Society Reviews*, 2020, **49**, 1688-1705.
8.      D. Larcher and J.-M. Tarascon, *Nature Chemistry*, 2015, **7**, 19-29.
9.      J. Hong, W. E. Gent, P. Xiao, K. Lim, D. H. Seo, J. Wu, P. M. Csernica, C. J. Takacs, D. Nordlund, C. J. Sun, K. H. Stone, D. Passarello, W. Yang, D. Prendergast, G. Ceder, M. F. Toney and W. C. Chueh, *Nature Materials*, 2019, **18**, 256-265.
10.     M. Saubanère, E. McCalla, J. M. Tarascon and M. L. Doublet, *Energy & Environmental Science*, 2016, **9**, 984-991.
11.     K. Kawai, X.-M. Shi, N. Takenaka, J. Jang, B. M. de Boisse, A. Tsuchimoto, D. Asakura, J. Kikkawa, M. Nakayama, M. Okubo and A. Yamada, *Energy & Environmental Science*, 2022, **15**, 2591-2600.
12.     J. Rana, J. K. Papp, Z. Lebens-Higgins, M. Zuba, L. A. Kaufman, A. Goel, R. Schmuch, M. Winter, M. S. Whittingham, W. Yang, B. D. McCloskey and L. F. J. Piper, *ACS Energy Letters*, 2020, **5**, 634-641.
13.     D. W. Dees, D. P. Abraham, W. Lu, K. G. Gallagher, M. Bettge and A. N. Jansen, *Journal of The Electrochemical Society*, 2015, **162**, A559-A572.
14.     G. Assat, C. Delacourt, D. A. D. Corte and J.-M. Tarascon, *Journal of The Electrochemical Society*, 2016, **163**, A2965-A2976.
15.     M. Sathiya, A. M. Abakumov, D. Foix, G. Rousse, K. Ramesha, M. Saubanère, M. L. Doublet, H. Vezin, C. P. Laisa, A. S. Prakash, D. Gonbeau, G. VanTendeloo and J. M. Tarascon, *Nature Materials*, 2015, **14**, 230-238.
16.     P. K. Nayak, J. Grinblat, M. Levi, E. Levi, S. Kim, J. W. Choi and D. Aurbach, *Advanced Energy Materials*, 2016, **6**, 1502398.
17.     D.-H. Seo, J. Lee, A. Urban, R. Malik, S. Kang and G. Ceder, *Nature Chemistry*, 2016, **8**, 692-697.
18.     R. A. House, U. Maitra, L. Jin, J. G. Lozano, J. W. Somerville, N. H. Rees, A. J. Naylor, L. C. Duda, F. Massel, A. V. Chadwick, S. Ramos, D. M. Pickup, D. E. McNally, X. Lu, T. Schmitt, M. R. Roberts and P. G. Bruce, *Chemistry of Materials*, 2019, **31**, 3293-3300.
19.     M. Ben Yahia, J. Vergnet, M. Saubanère and M.-L. Doublet, *Nature Materials*, 2019, **18**, 496-502.
20.     D. Y. W. Yu, K. Yanagida, Y. Kato and H. Nakamura, *Journal of The Electrochemical Society*, 2009, **156**, A417.
21.     J. Ahn, D. Chen and G. Chen, *Advanced Energy Materials*, 2020, **10**, 2001671.
22.     G. Assat, D. Foix, C. Delacourt, A. Iadecola, R. Dedryvere and J. M. Tarascon, *Nature Communications*, 2017, **8**, 2219.
23.     Y.-C. Lu and Y. Shao-Horn, *The Journal of Physical Chemistry Letters*, 2013, **4**, 93-99.
24.     J. Christensen, P. Albertus, R. S. Sanchez-Carrera, T. Lohmann, B. Kozinsky, R. Liedtke, J. Ahmed and A. Kojic, *Journal of The Electrochemical Society*, 2011, **159**, R1-R30.
25.     N. Zhang, X. Feng, D. Rao, X. Deng, L. Cai, B. Qiu, R. Long, Y. Xiong, Y. Lu and Y. Chai, *Nature Communications*, 2020, **11**, 4066.
26.     A. van Bommel and J. R. Dahn, *Electrochemical and Solid-State Letters*, 2010, **13**, A62.
27.     L. Wang, T. Liu, A. Dai, V. De Andrade, Y. Ren, W. Xu, S. Lee, Q. Zhang, L. Gu, S. Wang, T. Wu, H. Jin and J. Lu, *Nature Communications*, 2021, **12**, 5370.
28.     H. Li, R. Fong, M. Woo, H. Ahmed, D.-H. Seo, R. Malik and J. Lee, *Joule*, 2022, **6**, 53-91.
29.     J. Huang, P. Zhong, Y. Ha, D.-H. Kwon, M. J. Crafton, Y. Tian, M. Balasubramanian, B. D. McCloskey, W. Yang and G. Ceder, *Nature Energy*, 2021, **6**, 706-714.
30.     Z. Zi, Y. Zhang, Y. Meng, G. Gao and P. Hou, *New Journal of Chemistry*, 2020, **44**, 8486-8493.

31. S. Shi, S. Zhang, Z. Wu, T. Wang, J. Zong, M. Zhao and G. Yang, *Journal of Power Sources*, 2017, **337**, 82-91.

32. F.-D. Yu, L.-F. Que, Z.-B. Wang, Y. Xue, Y. Zhang, B.-S. Liu and D.-M. Gu, *Journal of Materials Chemistry A*, 2017, **5**, 9365-9376.

33. M. Park, X. Zhang, M. Chung, G. B. Less and A. M. Sastry, *Journal of Power Sources*, 2010, **195**, 7904-7929.

34. L. Zhang, N. Li, B. Wu, H. Xu, L. Wang, X.-Q. Yang and F. Wu, *Nano Letters*, 2015, **15**, 656-661.

35. M. Xu, L. Fei, W. Zhang, T. Li, W. Lu, N. Zhang, Y. Lai, Z. Zhang, J. Fang, K. Zhang, J. Li and H. Huang, *Nano Letters*, 2017, **17**, 1670-1677.

36. Q.-Q. Qiao, L. Qin, G.-R. Li, Y.-L. Wang and X.-P. Gao, *Journal of Materials Chemistry A*, 2015, **3**, 17627-17634.

37. Y. Ma, P. Liu, Q. Xie, G. Zhang, H. Zheng, Y. Cai, Z. Li, L. Wang, Z.-Z. Zhu, L. Mai and D.-L. Peng, *Nano Energy*, 2019, **59**, 184-196.

38. A. J. Perez, Q. Jacquet, D. Batuk, A. Iadecola, M. Saubanère, G. Rousse, D. Larcher, H. Vezin, M.-L. Doublet and J.-M. Tarascon, *Nature Energy*, 2017, **2**, 954-962.

39. N. Yabuuchi, Y. Tahara, S. Komaba, S. Kitada and Y. Kajiya, *Chemistry of Materials*, 2016, **28**, 416-419.

40. G. Assat and J.-M. Tarascon, *Nature Energy*, 2018, **3**, 373-386.

41. C. Zhao, Q. Wang, Y. Lu, L. Jiang, L. Liu, X. Yu, L. Chen, B. Li and Y.-S. Hu, *Energy Storage Materials*, 2019, **20**, 395-400.

42. X. Zhang, Y. Qiao, S. Guo, K. Jiang, S. Xu, H. Xu, P. Wang, P. He and H. Zhou, *Advanced Materials*, 2019, **31**, 1807770.

43. N. Voronina and S.-T. Myung, *Energy Material Advances*, 2021, **7**, 9-15.

44. H. Zheng, C. Zhang, Y. Zhang, L. Lin, P. Liu, L. Wang, Q. Wei, J. Lin, B. Sa and Q. Xie, *Advanced Functional Materials*, 2021, **31**, 2100783.

45. Q. Wang, S. Mariyappan, G. Rousse, A. V. Morozov, B. Porcheron, R. Dedryvère, J. Wu, W. Yang, L. Zhang, M. Chakir, M. Avdeev, M. Deschamps, Y.-S. Yu, J. Cabana, M.-L. Doublet, A. M. Abakumov and J.-M. Tarascon, *Nature Materials*, 2021, **20**, 353-361.

46. E. de la Llave, E. Talaie, E. Levi, P. K. Nayak, M. Dixit, P. T. Rao, P. Hartmann, F. Chesneau, D. T. Major, M. Greenstein, D. Aurbach and L. F. Nazar, *Chemistry of Materials*, 2016, **28**, 9064-9076.

47. D. Kim, M. Cho and K. Cho, *Advanced Materials*, 2017, **29**, 1701788.

48. H. Li, X. Zhao, Y. Li, Y. Gan, W. Qiu, J. Wang and J. Liu, *Journal of Materials Chemistry A*, 2021, **9**, 10364-10373.

49. U. Maitra, R. A. House, J. W. Somerville, N. Tapia-Ruiz, J. G. Lozano, N. Guerrini, R. Hao, K. Luo, L. Jin, M. A. Pérez-Osorio, F. Massel, D. M. Pickup, S. Ramos, X. Lu, D. E. McNally, A. V. Chadwick, F. Giustino, T. Schmitt, L. C. Duda, M. R. Roberts and P. G. Bruce, *Nature Chemistry*, 2018, **10**, 288-295.

50. W. Zheng, Q. Liu, Z. Wang, Z. Wu, S. Gu, L. Cao, K. Zhang, J. Fransaer and Z. Lu, *Energy Storage Materials*, 2020, **28**, 300-306.

51. X. Bai, M. Sathiya, B. Mendoza-Sánchez, A. Iadecola, J. Vergnet, R. Dedryvère, M. Saubanère, A. M. Abakumov, P. Rozier and J.-M. Tarascon, *Advanced Energy Materials*, 2018, **8**, 1802379.

52. J.-H. Song, G. Yoon, B. Kim, D. Eum, H. Park, D.-H. Kim and K. Kang, *Advanced Energy Materials*, 2020, **10**, 2001207.

53. M. Sathiya, G. Rousse, K. Ramesha, C. P. Laisa, H. Vezin, M. T. Sougrati, M. L. Doublet, D. Foix, D. Gonbeau, W. Walker, A. S. Prakash, M. Ben Hassine, L. Dupont and J. M. Tarascon, *Nature Materials*, 2013, **12**, 827-835.

54. B. Li, M. T. Sougrati, G. Rousse, A. V. Morozov, R. Dedryvère, A. Iadecola, A. Senyshyn, L. Zhang, A. M. Abakumov, M.-L. Doublet and J.-M. Tarascon, *Nature Chemistry*, 2021, **13**, 1070-1080.

55. M. D. Radin, J. Vinckeviciute, R. Seshadri and A. Van der Ven, *Nature Energy*, 2019, **4**, 639-646.

56. Y. Zuo, H. Shang, J. Hao, J. Song, F. Ning, K. Zhang, L. He and D. Xia, *Journal of the American Chemical Society*, 2023, **145**, 5174-5182.

57. J. Vinckeviciute, D. A. Kitchaev and A. Van der Ven, *Chemistry of Materials*, 2021, **33**, 1625-1636.

58. B. Li, Z. Zhuo, L. Zhang, A. Iadecola, X. Gao, J. Guo, W. Yang, A. V. Morozov, A. M. Abakumov and J.-M. Tarascon, *Nature Materials*, 2023, **22**, 1370-1379.

59. Y. Xie, M. Saubanère and M. L. Doublet, *Energy & Environmental Science*, 2017, **10**, 266-274.

60. K. Dai, J. Wu, Z. Zhuo, Q. Li, S. Sallis, J. Mao, G. Ai, C. Sun, Z. Li, W. E. Gent, W. C. Chueh, Y.-d. Chuang, R. Zeng, Z.-x. Shen, F. Pan, S. Yan, L. F. J. Piper, Z. Hussain, G. Liu and W. Yang, *Joule*, 2019, **3**, 518-541.

61. R. A. House, J.-J. Marie, J. Park, G. J. Rees, S. Agrestini, A. Nag, M. Garcia-Fernandez, K.-J. Zhou and P. G. Bruce, *Nature Communications*, 2021, **12**, 2975.

62. R. A. House, G. J. Rees, M. A. Pérez-Osorio, J.-J. Marie, E. Boivin, A. W. Robertson, A. Nag, M. Garcia-Fernandez, K.-J. Zhou and P. G. Bruce, *Nature Energy*, 2020, **5**, 777-785.

63. G. Assat, S. L. Glazier, C. Delacourt and J.-M. Tarascon, *Nature Energy*, 2019, **4**, 647-656.

64. B. Kim, J.-H. Song, D. Eum, S. Yu, K. Oh, M. H. Lee, H.-Y. Jang and K. Kang, *Nature Sustainability*, 2022, **5**, 708-716.

65. Z. Chen, J. Li and X. C. Zeng, *Journal of the American Chemical Society*, 2019, **141**, 10751-10759.

66. D. Eum, B. Kim, J.-H. Song, H. Park, H.-Y. Jang, S. J. Kim, S.-P. Cho, M. H. Lee, J. H. Heo, J. Park, Y. Ko, S. K. Park, J. Kim, K. Oh, D.-H. Kim, S. J. Kang and K. Kang, *Nature Materials*, 2022, **21**, 664-672.

67. T. Sudayama, K. Uehara, T. Mukai, D. Asakura, X.-M. Shi, A. Tsuchimoto, B. Mortemard de Boisse, T. Shimada, E. Watanabe, Y. Harada, M. Nakayama, M. Okubo and A. Yamada, *Energy & Environmental Science*, 2020, **13**, 1492-1500.

68. M. Okubo and A. Yamada, *ACS Applied Materials & Interfaces*, 2017, **9**, 36463-36472.

69. K. Zhang, Z. Jiang, F. Ning, B. Li, H. Shang, J. Song, Y. Zuo, T. Yang, G. Feng, X. Ai and D. Xia, *Advanced Energy Materials*, 2021, **11**, 2100892.

70. J. Chen, H. Chen, W. Deng, X. Gao, S. Yin, Y. Mei, S. Zhang, L. Ni, J. Gao, H. Liu, Y. Tian, L. Yang, X. Deng, G. Zou, H. Hou, J. Xie and X. Ji, *Energy Storage Materials*, 2022, **51**, 671-682.

71. R. A. House, G. J. Rees, K. McColl, J.-J. Marie, M. Garcia-Fernandez, A. Nag, K.-J. Zhou, S. Cassidy, B. J. Morgan, M. Saiful Islam and P. G. Bruce, *Nature Energy*, 2023, **8**, 351-360.

72. Y.-J. Park and D.-H. Seo, *Nature Energy*, 2023, **8**, 323-324.

73. D. A. Kitchaev, J. Vinckeviciute and A. Van der Ven, *Journal of the American Chemical Society*, 2021, **143**, 1908-1916.

74. I. I. Abate, C. D. Pemmaraju, S. Y. Kim, K. H. Hsu, S. Sainio, B. Moritz, J. Vinson, M. F. Toney, W. Yang, W. E. Gent, T. P. Devereaux, L. F. Nazar and W. C. Chueh, *Energy & Environmental Science*, 2021, **14**, 4858-4867.

75. A. Tsuchimoto, X.-M. Shi, K. Kawai, B. Mortemard de Boisse, J. Kikkawa, D. Asakura, M. Okubo and A. Yamada, *Nature Communications*, 2021, **12**, 631.

76. M. Okubo, K. Kawai, Z. Ma and A. Yamada, *Accounts of Materials Research*, 2022, **3**, 33-41.

77. Z. Zhang, D. Wu, X. Zhang, X. Zhao, H. Zhang, F. Ding, Z. Xie and Z. Zhou, *Journal of Materials Chemistry A*, 2017, **5**, 12752-12756.

78. M. S. Whittingham, *Journal of The Electrochemical Society*, 1976, **123**, 315.

79. W. E. Gent, K. Lim, Y. Liang, Q. Li, T. Barnes, S.-J. Ahn, K. H. Stone, M. McIntire, J. Hong, J. H. Song, Y. Li, A. Mehta, S. Ermon, T. Tyliszczak, D. Kilcoyne, D. Vine, J.-H. Park, S.-K. Doo, M. F. Toney, W. Yang, D. Prendergast and W. C. Chueh, *Nature Communications*, 2017, **8**, 2091.

80. T. Liu, J. Liu, L. Li, L. Yu, J. Diao, T. Zhou, S. Li, A. Dai, W. Zhao, S. Xu, Y. Ren, L. Wang, T. Wu, R. Qi, Y. Xiao, J. Zheng, W. Cha, R. Harder, I. Robinson, J. Wen, J. Lu, F. Pan and K. Amine, *Nature*, 2022, **606**, 305-312.

81. B. Mortemard de Boisse, M. Reynaud, J. Ma, J. Kikkawa, S.-i. Nishimura, M. Casas-Cabanas, C. Delmas, M. Okubo and A. Yamada, *Nature Communications*, 2019, **10**, 2185.

82. A. Gao, Q. Zhang, X. Li, T. Shang, Z. Tang, X. Lu, Y. Luo, J. Ding, W. H. Kan, H. Chen, W. Yin, X. Wang, D. Xiao, D. Su, H. Li, X. Rong, X. Yu, Q. Yu, F. Meng, C. Nan, C. Delmas, L. Chen, Y.-S. Hu and L. Gu, *Nature Sustainability*, 2022, **5**, 214-224.

83. D. Eum, B. Kim, S. J. Kim, H. Park, J. Wu, S. P. Cho, G. Yoon, M. H. Lee, S. K. Jung, W. Yang, W. M. Seong, K. Ku, O. Tamwattana, S. K. Park, I. Hwang and K. Kang, *Nature Materials*, 2020, **19**, 419-427.

84. N. Yabuuchi, *Nature Materials*, 2020, **19**, 372-373.

85. D. Luo, H. Zhu, Y. Xia, Z. Yin, Y. Qin, T. Li, Q. Zhang, L. Gu, Y. Peng, J. Zhang, K. M. Wiaderek, Y. Huang, T. Yang, Y. Tang, S. Lan, Y. Ren, W. Lu, C. M. Wolverton and Q. Liu, *Nature Energy*, 2023, **8**, 1078-1087.

86. B. Zhang, Y. Zhang, X. Wang, H. Liu, Y. Yan, S. Zhou, Y. Tang, G. Zeng, X. Wu, H.-G. Liao, Y. Qiu, H. Huang, L. Zheng, J. Xu, W. Yin, Z. Huang, Y. Xiao, Q. Xie, D.-L. Peng, C. Li, Y. Qiao and S.-G. Sun, *Journal of the American Chemical Society*, 2023, **145**, 8700-8713.

87. Q. Li, G. Li, C. Fu, D. Luo, J. Fan and L. Li, *ACS Applied Materials & Interfaces*, 2014, **6**, 10330-10341.

88. R. P. Qing, J. L. Shi, D. D. Xiao, X. D. Zhang, Y. X. Yin, Y. B. Zhai, L. Gu and Y. G. Guo, *Advanced Energy Materials*, 2016, **6**, 1501914.

89. C. Zhao, C. Chen, B. Hu, W. Tong, H. Liu, B. Hu and C. Li, *Chemistry of Materials*, 2022, **34**, 9240-9250.

90. B. Song, W. Li, P. Yan, S.-M. Oh, C.-M. Wang and A. Manthiram, *Journal of Power Sources*, 2016, **325**, 620-629.

91. C. Yin, L. Wan, B. Qiu, F. Wang, W. Jiang, H. Cui, J. Bai, S. Ehrlich, Z. Wei and Z. Liu, *Energy Storage Materials*, 2021, **35**, 388-399.

92. J. Vergnet, M. Saubanère, M.-L. Doublet and J.-M. Tarascon, *Joule*, 2020, **4**, 420-434.

93. X. Rong, J. Liu, E. Hu, Y. Liu, Y. Wang, J. Wu, X. Yu, K. Page, Y.-S. Hu, W. Yang, H. Li, X.-Q. Yang, L. Chen and X. Huang, *Joule*, 2018, **2**, 125-140.

94. R. M. Pasquarelli, D. S. Ginley and R. O'Hayre, *Chemical Society Reviews*, 2011, **40**, 5406-5441.

95. H. Ren, Y. Li, Q. Ni, Y. Bai, H. Zhao and C. Wu, *Advanced Materials*, 2021, **34**, 2106171.

96. X. L. Li, T. Wang, Y. Yuan, X. Y. Yue, Q. C. Wang, J. Y. Wang, J. Zhong, R. Q. Lin, Y. Yao and X. J. Wu, *Advanced Materials*, 2021, **33**, 2008194.

97. J. Liu, R. Qi, C. Zuo, C. Lin, W. Zhao, N. Yang, J. Li, J. Lu, X. Chen, J. Qiu, M. Chu, M. Zhang, C. Dong, Y. Xiao, H. Chen and F. Pan, *Nano Energy*, 2021, **88**, 106252.

98. C. Cheng, C. Chen, S. Chu, H. Hu, T. Yan, X. Xia, X. Feng, J. Guo, D. Sun, J. Wu, S. Guo and L. Zhang, *Advanced Materials*, 2022, **34**, 2201152.

99. Q. Jacquet, A. Perez, D. Batuk, G. Van Tendeloo, G. Rousse and J.-M. Tarascon, *Chemistry of Materials*, 2017, **29**, 5331-5343.

100. N. Yabuuchi, M. Nakayama, M. Takeuchi, S. Komaba, Y. Hashimoto, T. Mukai, H. Shiiba, K. Sato, Y. Kobayashi, A. Nakao, M. Yonemura, K. Yamanaka, K. Mitsuhara and T. Ohta, *Nature Communications*, 2016, **7**, 13814.

101. N. Luo, Z. Hou, C. Zheng, Y. Zhang, A. Stein, S. Huang and D. G. Truhlar, *Chemistry of Materials*, 2021, **33**, 834-844.

102. Q.-Q. Qiao, L. Qin, G.-R. Li, Y.-L. Wang and X.-P. Gao, *Journal of Materials Chemistry A*, 2015, **3**, 17627-17634.

103. Z. N. Taylor, A. J. Perez, J. A. Coca-Clemente, F. Braga, N. E. Drewett, M. J. Pitcher, W. J. Thomas, M. S. Dyer, C. Collins, M. Zanella, T. Johnson, S. Day, C. Tang, V. R. Dhanak, J. B. Claridge, L. J. Hardwick and M. J. Rosseinsky, *Journal of the American Chemical Society*, 2019, **141**, 7333-7346.

104. K. Yamamoto, Y. Zhou, N. Yabuuchi, K. Nakanishi, T. Yoshinari, T. Kobayashi, Y. Kobayashi, R. Yamamoto, A. Watanabe, Y. Orikasa, K. Tsuruta, J. Park, H. R. Byon, Y. Tamenori, T. Ohta and Y. Uchimoto, *Chemistry of Materials*, 2020, **32**, 139-147.

105. J. Lee, S. Koo, J. Lee and D. Kim, *Journal of Materials Chemistry A*, 2021, **9**, 11762-11770.

106. D. Chen, J. Wu, J. K. Papp, B. D. McCloskey, W. Yang and G. Chen, *Small*, 2020, **16**, 2000656.

107. M. Cho, S. H. Song, S. Hong, K. S. Kim, M. Avdeev, J. G. Yoo, K. T. Ko, J. Hong, J. Kim and S. Lee, *Small*, 2021, **17**, 2100840.

108. J. Lee, S. Park, G. Choi, D. Kwon, J. Kim, H. Kim, M. Cho and D. Kim, *Advanced Energy Materials*, 2022, **12**, 2201319.

109. M. Cho, S. H. Song, S. Hong, K. S. Kim, M. Avdeev, J.-G. Yoo, K.-T. Ko, J. Hong, J. Kim, S. Lee and H. Kim, *Small*, 2021, **17**, 2100840.

110. Z. Deng and A. Manthiram, *The Journal of Physical Chemistry C*, 2011, **115**, 7097-7103.

111. W. Tang, A. Li, G. Zhou, Z. Chen, Z. Yang, J. Su and W. Zhang, *ACS Applied Materials & Interfaces*, 2022, **14**, 38865-38874.

112. K. Luo, M. R. Roberts, R. Hao, N. Guerrini, D. M. Pickup, Y.-S. Liu, K. Edström, J. Guo, A. V. Chadwick, L. C. Duda and P. G. Bruce, *Nature Chemistry*, 2016, **8**, 684-691.

113. C. Zhao, H. Liu, F. Geng, B. Hu and C. Li, *Energy Storage Materials*, 2022, **48**, 290-296.

114. Z. Lu, D. D. MacNeil and J. R. Dahn, *Electrochemical and Solid-State Letters*, 2001, **4**, A191.

115. Z. Lu and J. R. Dahn, *Journal of The Electrochemical Society*, 2002, **149**, A815.

116. A. D. Robertson and P. G. Bruce, *Chemistry of Materials*, 2003, **15**, 1984-1992.

117. E. Hu, X. Yu, R. Lin, X. Bi, J. Lu, S. Bak, K.-W. Nam, H. L. Xin, C. Jaye, D. A. Fischer, K. Amine and X.-Q. Yang, *Nature Energy*, 2018, **3**, 690-698.

118. C. Zhan, Z. Yao, J. Lu, L. Ma, V. A. Maroni, L. Li, E. Lee, E. E. Alp, T. Wu, J. Wen, Y. Ren, C. Johnson, M. M. Thackeray, M. K. Y. Chan, C. Wolverton and K. Amine, *Nature Energy*, 2017, **2**, 963-971.

119. C. P. Laisa, A. K. Nanda Kumar, S. Selva Chandrasekaran, P. Murugan, N. Lakshminarasimhan, R. Govindaraj and K. Ramesha, *Journal of Power Sources*, 2016, **324**, 462-474.

120. D. Dixon, S. Mangold, M. Knapp, H. Ehrenberg and A. Bhaskar, *Advanced Energy Materials*, 2021, **11**, 2100479.

121. Y. Zhang, M. Wu, J. Ma, G. Wei, Y. Ling, R. Zhang and Y. Huang, *ACS Central Science*, 2020, **6**, 232-240.

122. N. Li, J. Wu, S. Hwang, J. K. Papp, W. H. Kan, L. Zhang, C. Zhu, B. D. McCloskey, W. Yang and W. Tong, *ACS Energy Letters*, 2020, **5**, 3535-3543.

123. Z. Zhu, A. Kushima, Z. Yin, L. Qi, K. Amine, J. Lu and J. Li, *Nature Energy*, 2016, **1**, 16111.

124. E. Boivin, N. Guerrini, R. A. House, J. G. Lozano, L. Jin, G. J. Rees, J. W. Somerville, C. Kuss, M. R. Roberts and P. G. Bruce, *Advanced Functional Materials*, 2021, **31**, 2003660.

125. H. Komatsu, T. Minato, T. Matsunaga, K. Shimoda, T. Kawaguchi, K. Fukuda, K. Nakanishi, H. Tanida, S. Kobayashi, T. Hirayama, Y. Ikuhara, H. Arai, Y. Ukyo, Y. Uchimoto, E. Matsubara and Z. Ogumi, *The Journal of Physical Chemistry C*, 2018, **122**, 20099-20107.

126. Y. Gong, X. Li, L. Zeng, Y. Huang, B. Qiu and Z. Liu, *The Journal of Physical Chemistry Letters*, 2023, **14**, 4575-4582.

127. E. J. Kim, L. A. Ma, L. C. Duda, D. M. Pickup, A. V. Chadwick, R. Younesi, J. T. S. Irvine and A. R. Armstrong, *ACS Applied Energy Materials*, 2020, **3**, 184-191.

128. B. Li, G. Rousse, L. Zhang, M. Avdeev, M. Deschamps, A. M. Abakumov and J.-M. Tarascon, *Energy & Environmental Science*, 2023, **16**, 1210-1222.

129. C.-G. Shi, X. Peng, P. Dai, P. Xiao, W.-C. Zheng, H.-Y. Li, H. Li, S. Indris, S. Mangold, Y.-H. Hong, C.-X. Luo, C.-H. Shen, Y.-M. Wei, L. Huang and S.-G. Sun, *Advanced Energy Materials*, 2022, **12**, 2200569.

130. W. Kong, D. Zhou, Q. Zhang, D. Wong, K. An, C. Schulz, N. Zhang, J. Zhang and X. Liu, *Advanced Functional Materials*, 2023, **33**, 2211033.

131. J. Li, C. Lin, M. Weng, Y. Qiu, P. Chen, K. Yang, W. Huang, Y. Hong, J. Li, M. Zhang, C. Dong, W. Zhao, Z. Xu, X. Wang, K. Xu, J. Sun and F. Pan, *Nature Nanotechnology*, 2021, **16**, 599-605.

132. W. Kong, J. Zhang, D. Wong, W. Yang, J. Yang, C. Schulz and X. Liu, *Angewandte Chemie International Edition*, 2021, **60**, 27102-27112.

133. G. Ceder, Y. M. Chiang, D. R. Sadoway, M. K. Aydinol, Y. I. Jang and B. Huang, *Nature*, 1998, **392**, 694-696.

134. Z. W. Lebens-Higgins, N. V. Faenza, M. D. Radin, H. Liu, S. Sallis, J. Rana, J. Vinckeviciute, P. J. Reeves, M. J. Zuba, F. Badway, N. Pereira, K. W. Chapman, T.-L. Lee, T. Wu, C. P. Grey, B. C. Melot, A. Van Der Ven, G. G. Amatucci, W. Yang and L. F. J. Piper, *Materials Horizons*, 2019, **6**, 2112-2123.

135. H. Zhang, H. Liu, L. F. J. Piper, M. S. Whittingham and G. Zhou, *Chemical Reviews*, 2022, **122**, 5641-5681.

136. Y. Chu, Y. Mu, L. Zou, Y. Hu, S. Kang, H. Ren, M. Han, Q. Zhang, L. Wei and L. Zeng, *Small Structures*, 2023, **n/a**, 2300247.

137. Z. Q. Deng and A. Manthiram, *The Journal of Physical Chemistry C*, 2011, **115**, 7097-7103.

138. X. Xiang, J. C. Knight, W. Li and A. Manthiram, *The Journal of Physical Chemistry C*, 2014, **118**, 21826-21833.

139. S. Li, Z. Liu, L. Yang, X. Shen, Q. Liu, Z. Hu, Q. Kong, J. Ma, J. Li, H.-J. Lin, C.-T. Chen, X. Wang, R. Yu, Z. Wang and L. Chen, *Nano Energy*, 2022, **98**, 107335.

140. B. Li, N. Jiang, W. Huang, H. Yan, Y. Zuo and D. Xia, *Advanced Functional Materials*, 2018, **28**, 1704864.

141. N. Yabuuchi, M. Takeuchi, M. Nakayama, H. Shiiba, M. Ogawa, K. Nakayama, T. Ohta, D. Endo, T. Ozaki, T. Inamasu, K. Sato and S. Komaba, *Proceedings of the National Academy of Sciences*, 2015, **112**, 7650-7655.

142. J. Xu, M. Sun, R. Qiao, S. E. Renfrew, L. Ma, T. Wu, S. Hwang, D. Nordlund, D. Su, K. Amine, J. Lu, B. D. McCloskey, W. Yang and W. Tong, *Nature Communications*, 2018, **9**, 947.

143. J. Wu, Z. Zhuo, X. Rong, K. Dai, Z. Lebens-Higgins, S. Sallis, F. Pan, L. F. J. Piper, G. Liu, Y.-d. Chuang, Z. Hussain, Q. Li, R. Zeng, Z.-x. Shen and W. Yang, *Science Advances*, 2020, **6**, eaaw3871.

144. L. Yao, P. Zou, C. Wang, J. Jiang, L. Ma, S. Tan, K. A. Beyer, F. Xu, E. Hu and H. L. Xin, *Advanced Energy Materials*, 2022, **12**, 2201989.

145. P. Zhou, Z. Che, J. Liu, J. Zhou, X. Wu, J. Weng, J. Zhao, H. Cao, J. Zhou and F. Cheng, *Energy Storage Materials*, 2023, **57**, 618-627.

146. Y. S. Meng, G. Ceder, C. P. Grey, W. S. Yoon, M. Jiang, J. Bréger and Y. Shao-Horn, *Chemistry of Materials*, 2005, **17**, 2386-2394.

147. X. Qi, X. Wu, L. Li, Y. Xiang, Y. Liu, K. Huang, E. Yuval, D. Aurbach and X. Zhang, *Advanced Energy Materials*, 2022, **12**, 2202355.

148. D. Eum, H.-Y. Jang, B. Kim, J. Chung, D. Kim, S.-P. Cho, S. H. Song, S. Kang, S. Yu, S.-O. Park, J.-H. Song, H. Kim, O. Tamwattana, D.-H. Kim, J. Lim and K. Kang, *Energy & Environmental Science*, 2023, **16**, 673-686.

149. E. Zhao, M. Zhang, X. Wang, E. Hu, J. Liu, X. Yu, M. Olguin, T. A. Wynn, Y. S. Meng and K. Page, *Energy Storage Materials*, 2020, **24**, 384-393.

150. R. A. House, U. Maitra, M. A. Perez-Osorio, J. G. Lozano, L. Jin, J. W. Somerville, L. C. Duda, A. Nag, A. Walters, K. J. Zhou, M. R. Roberts and P. G. Bruce, *Nature*, 2020, **577**, 502-508.

151. J. Lee, A. Urban, X. Li, D. Su, G. Hautier and G. Ceder, *Science*, 2014, **343**, 519-522.

152. S. Myeong, W. Cho, W. Jin, J. Hwang, M. Yoon, Y. Yoo, G. Nam, H. Jang, J.-G. Han, N.-S. Choi, M. G. Kim and J. Cho, *Nature Communications*, 2018, **9**, 3285.

153. J. Lee, D. Yu, Z. Zhu, X. Yao, C. Wang, Y. Dong, R. Malik and J. Li, *ACS Applied Energy Materials*, 2020, **3**, 7931-7943.

154. J. Lee, D. A. Kitchaev, D.-H. Kwon, C.-W. Lee, J. K. Papp, Y.-S. Liu, Z. Lun, R. J. Clément, T. Shi, B. D. McCloskey, J. Guo, M. Balasubramanian and G. Ceder, *Nature*, 2018, **556**, 185-190.

155. W. D. Richards, S. T. Dacek, D. A. Kitchaev and G. Ceder, *Advanced Energy Materials*, 2018, **8**, 1701533.

156. H. Ji, J. Wu, Z. Cai, J. Liu, D.-H. Kwon, H. Kim, A. Urban, J. K. Papp, E. Foley, Y. Tian, M. Balasubramanian, H. Kim, R. J. Clément, B. D. McCloskey, W. Yang and G. Ceder, *Nature Energy*, 2020, **5**, 213-221.

157. W. Jin, S. Myeong, J. Hwang, H. Jang, J. Sung, Y. Yoo, M. G.

Kim and J. Cho, *Advanced Energy Materials*, 2020, **10**, 1904092.

158. H. Ji, A. Urban, D. A. Kitchaev, D.-H. Kwon, N. Artrith, C. Ophus, W. Huang, Z. Cai, T. Shi, J. C. Kim, H. Kim and G. Ceder, *Nature Communications*, 2019, **10**, 592.

159. Z. Lun, B. Ouyang, D.-H. Kwon, Y. Ha, E. E. Foley, T.-Y. Huang, Z. Cai, H. Kim, M. Balasubramanian, Y. Sun, J. Huang, Y. Tian, H. Kim, B. D. McCloskey, W. Yang, R. J. Clément, H. Ji and G. Ceder, *Nature Materials*, 2021, **20**, 214-221.

160. B. Mortemard de Boisse, S. i. Nishimura, E. Watanabe, L. Lander, A. Tsuchimoto, J. Kikkawa, E. Kobayashi, D. Asakura, M. Okubo and A. Yamada, *Advanced Energy Materials*, 2018, **8**, 1800409.

161. B. Song, M. Tang, E. Hu, O. J. Borkiewicz, K. M. Wiaderek, Y. Zhang, N. D. Phillip, X. Liu, Z. Shadike, C. Li, L. Song, Y.-Y. Hu, M. Chi, G. M. Veith, X.-Q. Yang, J. Liu, J. Nanda, K. Page and A. Huq, *Chemistry of Materials*, 2019, **31**, 3756-3765.